NASA CR-165151
GDC-CRAD-80-014

(NASA-CR-165151) COMPARATIVE THERMAL ANALYSIS OF ALTERNATE CRYOGENIC FLUID MANAGEMENT EXPERIMENT (CFME) CONFIGURATIONS (General Dynamics/Convair) 65 p
HC A04/MF A01
CSCL 22A G3/12

N80-32412

Unclas
28806

COMPARATIVE THERMAL ANALYSIS OF ALTERNATE CRYOGENIC FLUID MANAGEMENT EXPERIMENT (CFME) CONFIGURATIONS

GENERAL DYNAMICS
Convair Division

NASA CR-165151
GDC-CRAD-80-014

COMPARATIVE THERMAL ANALYSIS OF ALTERNATE CRYOGENIC FLUID MANAGEMENT EXPERIMENT (CFME) CONFIGURATIONS

July 1980

Prepared by
F. Merino
R.F. O'Neill

Prepared for
National Aeronautics and Space Administration
LEWIS RESEARCH CENTER
21000 Brookpark Road
Cleveland, Ohio 44135

Prepared Under
Contract NAS3-21935

Prepared by
GENERAL DYNAMICS CONVAIR DIVISION
P.O. Box 80847
San Diego, California 92138

FOREWORD

The following final report summarizes the Task V and VI technical effort conducted under Contract NAS3-21935 by the General Dynamics Convair Division from February, 1980 to June, 1980. The original Contract was amended to include the thermal analysis of alternate Cryogenic Fluid Management Experiment (CFME) configurations for comparison with the baseline being developed by Martin-Marietta Company under Contract NAS3-21591. The contract was administered by the National Aeronautics and Space Administration, Lewis Research Center, Cleveland, Ohio.

NASA/LeRC Program Manager - E. P. Symons

Task Leader - F. Merino

Assisting - R. F. O'Neill

All data are presented with the International System of Units as the primary system and English Units as the secondary system. The English system was used for the basic calculations.

TABLE OF CONTENTS

PRECEDING PAGE BLANK NOT FILMED

TABLE OF CONTENTS, Contd.

LIST OF FIGURES

LIST OF FIGURES, Contd

LIST OF TABLES

SUMMARY

An analytical study of the Cryogenic Fluid Management Experiment (CFME) was conducted in which alternate Thermodynamic Vent Systems (TVS) were incorporated into the baseline CFME insulation and pressure control system. Work performed under NASA/Martin Marietta Contract NAS3-21591, as described in the Conceptual Design, Thermal, and Hydrodynamic Reports, identifies the baseline CFME configuration. A systems comparison of the baseline CFME, including thermodynamic performance, was then made with our own analysis data for the alternate CFME system.

The baseline CFME incorporates a vapor-cooled shield (VCS) as a major subcomponent of its insulation and pressure control system. The VCS is cooled by vent flow from the CFME pressure vessel. It functions as a heat exchanger, intercepting a portion of the energy admitted through the multilayer insulation (MLI) blanket. The VCS achieves the benefit of reduced LH_2 boiloff and accompanying pressure decrease at the expense of VCS weight, complexity, and cost. However, it is conceivable that tolerable boiloff and pressure levels can be maintained throughout the 7-day on-orbit storage period without the use of a VCS in the CFME insulation and pressure control system. The analytical investigation of the feasibility and advisability of deleting the VCS was the subject of this study.

Two alternate concepts of CFME insulation and pressure control, neither of which incorporated the VCS, were investigated. The first concept employed a Thermodynamic Vent System (TVS) to throttle the flow through a heat exchanger in the interior of the pressure vessel to decrease boiloff and pressure rise rate, while the second concept utilized a TVS without an internal heat exchanger. Both concepts employed the cold-side fluid to intercept penetration heat leaks. Cold side fluid was provided from the liquid acquisition device. The steady-state heating environment and mission schedule imposed upon this study are given in Figures 1-2 and 1-3.

A thermodynamic evaluation of the second concept revealed that it was not a viable alternative. The imposed constraint, that it not be mounted to the internal nor external walls of the pressure vessel, rendered it incapable of extracting sufficient energy from propellants to achieve pressure control.

A conceptual design of the internal heat exchanger was developed for the first TVS concept. Sizing was based upon the thermal analysis described in Section 2.7. Design and installation details are given in Figure 4-1, 4-2 and 4-3. TVS performance with this internal HX was assessed for the seven-day mission. Both CFME pressure control and vent mass requirements were determined and compared to the baseline configuration. The following results were obtained:

a. The alternate configuration should have greater pressure control capability than the baseline.

b. Either concept will perform satisfactorily during the seven-day mission. This is due both to the positive and negative influences of the VCS. Steady-state VCS performance will exceed that of the internal HX. However, the VCS thermal mass represents an additional heat source that penalizes the baseline configuration.

The baseline and alternate configurations were also compared on the basis of development, fabrication, installation and complexity. The simpler internal HX installation was rated favorably in each area, which led to the conclusion that VCS development costs would be greater.

Based upon the above comparisons, the internal heat exchanger was recommended as a replacement for the vapor-cooled shield.

1

INTRODUCTION

An analytical study of the Cryogenic Fluid Management Experiment (CFME) was conducted in an alternate configuration in which a vapor-cooled shield (VCS) was not incorporated in the CFME insulation and pressure-control system. The study objective was to identify a simple, lightweight alternative to the baseline CFME thermal-control system.

1.1 BACKGROUND

The Cryogenic Fluid Management Experiment (CFME) is a lightweight, modular Spacelab experiment for advancing the technology of on-orbit storage and supply of sub-critical cryogenic fluids. It is designed for installation on a Spacelab pallet in the Shuttle Orbiter payload bay. The CFME will combine an efficient thermal-control system and a fine-mesh screen fluid-acquisition device to permit long-term storage, and delivery on demand, of vapor-free cryogens in a space environment.

In the recent past, a shift in emphasis of CFME mission requirements has occurred. It had been determined that long-term storage (of many weeks duration) was no longer a major design driver. Rather, the CFME mission duration would be limited to approximately one week. Specifically, the CFME was to be considered as a storage and supply system for OTV- related fluid management experiments.

In light of the reduced-on-orbit storage requirements, the high thermal performance provided by the VCS would be no longer essential. The possibility existed that the high thermal performance of the VCS could not be justified on the basis of boiloff reduction. That is, given the seven day mission duration, perhaps a lightweight alternative, even with increased boiloff, would provide adequate thermal protection and pressure control. This alternative configuration would be especially appealing if it resulted in a less complex CFME design and development program.

1.1.1 BASELINE CFME CONFIGURATION. The CFME conceptual design has been set forth in Reference 1-1. Thermal and hydrodynamic analyses of the CFME are contained in References 1-2 and 1-3. A simplified illustration of the baseline CFME is presented in Figure 1-1, in which detail is limited to the major structural and thermal control elements of the experiment:

1.1.1.1 Pressure Vessel. The 106-cm (41.7-inch) pressure vessel can contain 600 liters of LH_2. Maximum operating pressure of the aluminum vessel is 410 kN/m^2 (60 psia).

1.1.1.2 Thermal Control System. A vapor-cooled shield is positioned immediately outboard of the pressure vessel. Heat is extracted from the shield by fluid lines containing vent flow from the thermodynamic vent system (TVS). Local heat exchangers at tank penetrations also contain vent flow from the TVS. A multilayer insulation (MLI) blanket resides outboard of the vapor-cooled shield.

1.1.1.3 Vacuum Jacket. The pressure vessel, TVS, and insulation are enclosed by a lightweight aluminum vacuum vessel, which contains mounting provisions for the internal tankage. The vacuum vessel permits tank thermal control during ground operation and ascent.

1.1.1.4 Liquid Acquisition. A fine-mesh screen liquid-acquisition device is incorporated in the pressure vessel to ensure expulsion of vapor-free LH_2. It is not shown in Figure 1-1.

1.1.1.5 Additional CFME Systems. Pressurization, data acquisition and control, and mass gauging are major CFME systems and functions which were not addressed in this study.

1.1.2 THERMAL PERFORMANCE. The baseline configuration includes an MLI blanket (75 layers) outboard of the VCS, as defined in Reference 1-1. The MLI is double-aluminized Mylar with double-layer separators of B4A Dacron mesh. The predicted steady-state heat flux, given in Reference 1-1, is shown in Figure 1-2 both with the TVS

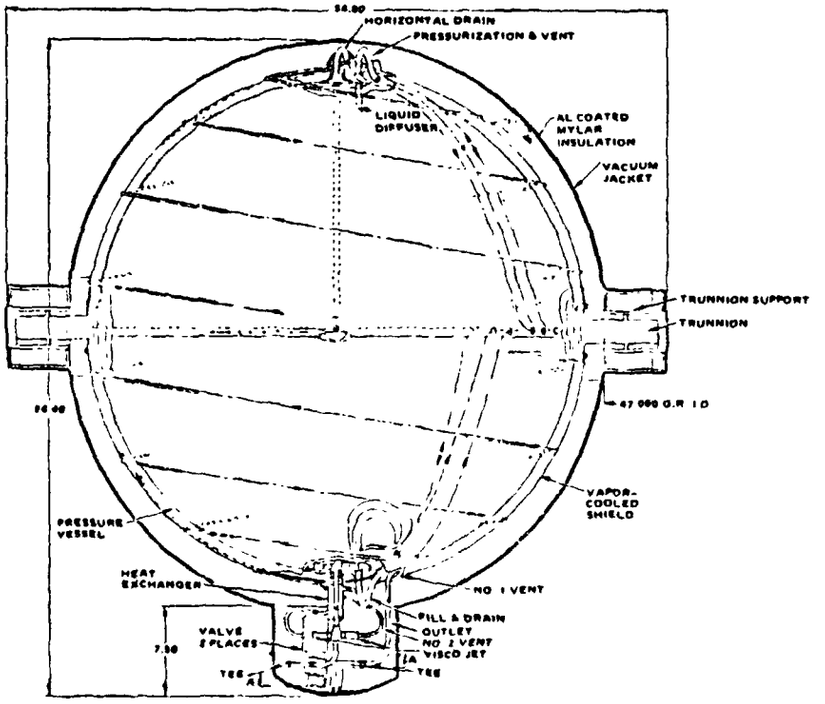

Pressure Vessel

Operating Pressure = 410 kN/m^2 (60 psia)
Volume = 0.62 m^3 (22 ft^3)

Thermal Control System

Vapor-Cooled Shield (VCS)
HX-1 (Operates Continuously)
HX-2 (Tank Pressure Controlled Operation)
Vacuum Jacket
MLI
Other (Liquid Acquisition Device, etc.)

Figure 1-1. Baseline CFME Configuration

TVS Not Operating				Watts Btu/hr		Percent
MLI				2.96	(10.1)	41.5
Supports	Fixed	0.90	(3.07)			
	Sliding	0.62	(2.10)	1.85	(6.32)	26.0
	Anti-Torsion	0.34	(1.15)			
Fill & Drain Line				0.22	(0.76)	3.1
Outflow Line				0.17	(0.58)	2.4
Pressurization and Vent Line				0.08	(0.28)	1.2
Horizontal Drain Line				0.27	(0.92)	3.8
Instrumentation Lead Wires (To Pressure Vessel)				0.69	(2.34)	9.6
Outflow Control Valve Lead Wires				0.04	(0.15)	0.6
Thermodynamic Vent Lines				0.84	(2.88)	11.8
			Total	7.13	(24.34) Btu/hr	100%

With TVS On

Net Heat Leak to Fluid + 2.4 Watts (+8.1 Btu/Hr) With HX-1 Only
- VCS Temp. 92K (165R)

Reference: MCR-79-564, June 1979

Figure 1-2. Steady-State Heating Environment (Baseline CFME)

not functioning and operating. Note that the net heat leak to liquid hydrogen can be reduced from 7.1 watts to 2.4 watts (24.34 Btu/hr to 8.1 Btu/hr) with HX No. 1 operating. The function of HX-1 and HX-2 and how they intercept heat is discussed below.

1.1.2.1 Thermodynamic Vent System Operation. The TVS consists of two heat exchanger systems (HX-1 and HX-2) that intercept heat input to the propellants when operating. HX-1 will operate continuously and HX-2 will be controlled on the basis of tank pressure, and will be cycled as required to maintain vessel pressure at a pre-determined level. Each heat exchanger draws liquid from the liquid acquisition device, which then flows through a viscojet, reducing pressure and temperature.

HX-1 withdraws heat from the penetrations at the bottom of the pressure vessel (outflow and fill-and-drain lines), then from the VCS, spirals from bottom to top, and finally is routed to intercept heat from the upper penetration lines. Hydrogen vapor will vent at a temperature of 92K (165R). Approximately 67 percent of the steady-state heat input rate will be intercepted by this heat exchanger.

HX-2 will be routed directly to the top penetrations, then to the VCS, spiralling downward, and finally will be routed along the outflow and fill-and-drain lines to their penetration of the vacuum jacket. This heat exchanger will provide the balance of the TVS heat intercept capability.

Transient heating rates occurring during cooldown of the vessel were not available for this study.

1.2 STUDY GROUNDRULES

The purpose of this study was to determine if an acceptable alternative to the baseline CFME thermal-control system could be identified. Specifically, the objective was to replace the VCS (because of its high weight and complex structure) with a simple and lightweight alternative system. Two alternative TVS configurations were specified by NASA/Lewis Research Center and are discussed in Sections 1.2.1 and 1.2.2. Each configuration would minimize any changes to the baseline CFME.

1.2.1 CONCEPT NO. 1. This concept includes two heat exchangers. HX-1 is external to the pressure vessel and will intercept all penetrations, including the major heating penetrations such as supports, trunnion, instrumentation lead wires and thermodynamic vent lines. As with the baseline configuration, liquid is supplied from the liquid-acquisition device and throttled through the viscojet. It was assumed that the propellant vent temperature would be equal to that of the stored liquid. A continuous vent flowrate of 0.032 kg/hr (0.0712 lb/hr) was selected to intercept the 4.17 watts (14.24 Btu/hr) of heating penetrations identified in Figure 1-2.

HX-2 will be internally mounted to the walls of the pressure vessel in order to extract energy from the tanked propellants. Liquid will be supplied from the liquid acquisition device and throttled to a reduced pressure and temperature by the viscojet before entering HX-2. A discussion of the method for extracting energy from the tank propellants is given in Sections 2.5 and 2.6. Flow through HX-2 will be activated by vessel pressure, as required to control propellant pressure. Pressure control is achieved by cooling the propellant, which can occur only if the propellant energy-removal rate exceeds the MLI heat-input rate (all other heat rates are intercepted by HX-1).

HX-2 was the only heat exchanger analyzed for this concept. HX-1 was not analyzed because it was beyond the scope of this study. It was, therefore, assumed that the alternative HX-1 configurations were equivalent to the baseline HX-1 configuration in terms of weight and complexity.

1.2.2 CONCEPT NO. 2. This concept also includes two heat exchangers. HX-1 is identical in every respect to the Concept No. 1 configuration. However, it was stipulated that HX-2 not be mounted inside the pressure vessel, and not be physically mounted to the external wall of the vessel. These conditions left only one alternative;

HX-2 will be similar to HX-1 in function and design. The implications of this design constraint are explored in Section 3.1.3.

1.2.3 CFME MISSION TIMELINES. The mission timeline selected for this study is depicted in Figure 1-3. This figure identifies typical CFME operational requirements of storage, thermal and pressure stabilization and propellant outflow. However, a determination had been made early in the study that an evaluation of propellant expulsion would not influence the comparative analysis of alternative thermal-control systems; this task was subsequently deleted.

1.2.4 CFME BOUNDARY CONDITIONS. Propellant pressure and temperature histories of a CFME mission will be heavily influenced by the prelaunch tanking schedule, as well as the steady-state heating environment. The propellant tanking schedule selected for the study is given in Table 1-1. Also included are assumptions related to heat exchanger operation, propellant state conditions and liquid-vapor distribution.

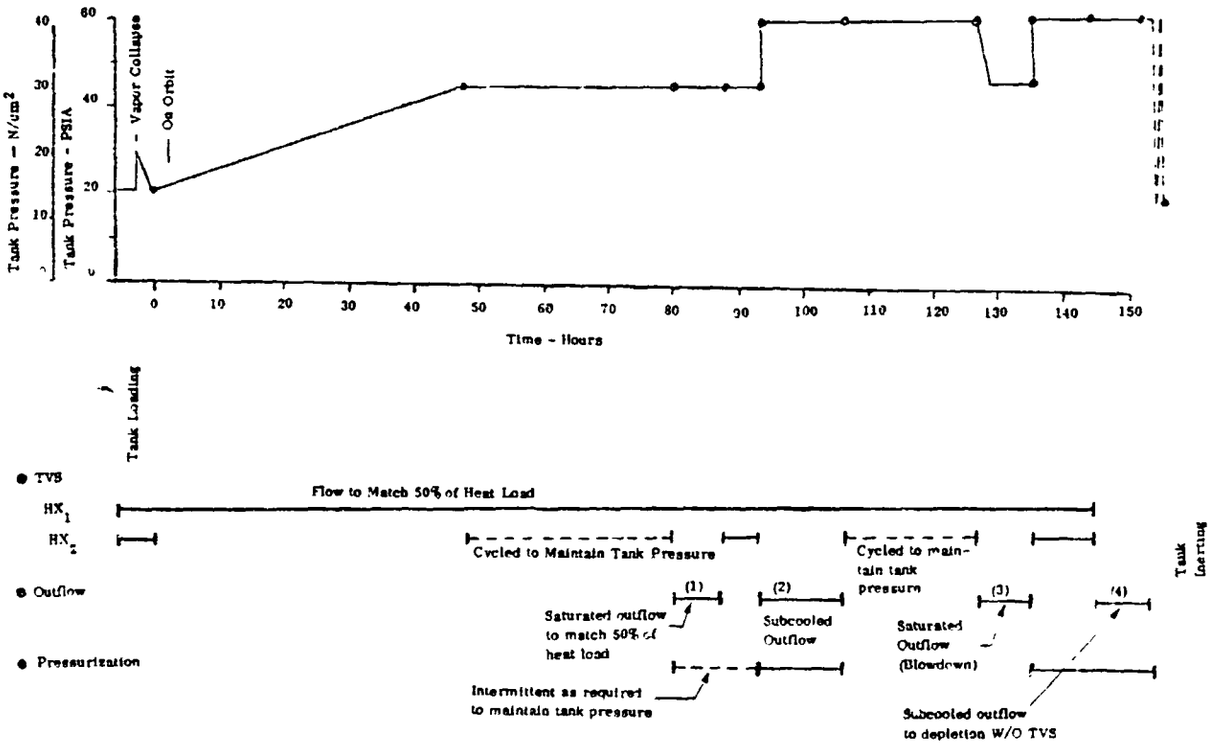

Mission Operation Requirements

Four-Day Storage and Stabilization Period
Four LH_2 Outflow Sequences to Demonstrate Stability

Figure 1-3. CFME Mission Timelines

Table 1-1. Selected CFME Mission Timelines and Assumed Conditions

1. Tank lockup at T-4 hours (start of system cooldown + 1.5 hours). HX-1 is activated.

2. Flat liquid-vapor interface exists until SSME cutoff (T + 8 minutes). Non-equilibrium pressure rise occurs during this period.

3. Propellant thermal equilibrium conditions will result from SSME cutoff disturbances. A zero-g liquid-vapor distribution will exist for remainder of mission.

4. Initiate constant pressure control when tank pressure increases to a pre-determined level (HX-2 will be activated).

5. Initiate constant-pressure liquid propellant expulsion. HX-2 turned off during liquid expulsion.

6. Mission ends at T + 168 hours.

2

ALTERNATE PRESSURE CONTROL SYSTEM THERMAL DESIGN ANALYSIS

2.1 THERMAL ANALYSIS OVERVIEW

2.1.1 ANALYSIS OBJECTIVES. Three major thermal analysis objectives are addressed in this investigation of CFME alternate pressure control systems:

a. Optimization of the multilayer insulation (MLI) thickness for employment with pressure control systems with, and/or without a heat exchanger in the pressure vessel interior.

b. Analytical prediction of the pressure vessel and tankage thermal response in all operational conditions to support assessment of the pressure control capabilities of the alternate systems.

c. Definition of a set of configuration data to support detail design of an internal heat exchanger.

2.1.2 THERMAL ANALYSIS RATIONALE. The following assumptions and thermal analysis guidelines have been employed in this study:

a. MLI material and lay-up methods are assumed to be as defined in Reference 1-1 for the baseline CMFE configuration. Only the blanket thickness will be subject to change.

b. Pressure vessel penetration heat leaks are assumed to be as defined in Reference 1-1, and local heat exchange devices employed at the baseline CFME penetrations are not addressed in this study. They are assumed to retain a baseline configuration, and to be accommodated by heat exchanger number one (HX-1) of the pressure control system.

c. The following operational CFME timelines are pertinent in terms of thermal boundary conditions employed in this study: CFME lockup at 1.5 hours after initial cooldown, and SSME shutdown at 14880 seconds (4.13 hours) after lockup. Convective heat transport in the tankage liquid and ullage was conservatively assumed to cease entirely at SSME shutdown. A flat surface liquid/ullage interface was assumed to exist prior to SSME shutdown.

2.1.3 THERMAL ANALYSIS SIMULATIONS. Six separate thermal-analytical simulations are included in this study:

a. A parametric, steady-state analysis of the MLI blanket installation over a range of blanket thickness and hot-side temperature values.

b. A transient analysis of an 84-layer MLI installation, yielding heat rate to the CFME pressure vessel as a function of time after initial cooldown.

c. A transient analysis of the flat-surface minimum ullage covering the interval, CFME lockup at cooldown plus 1.5 hours through SSME shutdown, 4.13 hours after lockup.

d. A transient analysis of the zero-g minimum ullage condition commencing at SSME shutdown, and including the effects of HX-2 heat extraction for pressure control, which commences approximately 67 hours later.

e. A steady-state analysis of the CFME pressure vessel and contents in a zero-g maximum ullage condition.

f. A steady-state analysis of a typical section of HX-2 surface and vent tubing, for calculation of an acceptable tube spacing and length.

Analyses a. thru d. above were multi-node numerical studies for which the general purpose computer program of Reference 2-1 was employed. Analysis e. above was performed with the aid of the Reference 2-2 computer program. Analysis f. above was amenable to closed-form solution of an ordinary differential equation.

2.2 PARAMETRIC ANALYSIS FOR MLI OPTIMIZATION

Removal of the VCS would result in a minimum radial dimension of 5.08 cm (2 in.) between the pressure vessel (girth ring) and the vacuum vessel. This would permit an increase in the baseline CFME MLI blanket thickness, which is defined in Reference 1-1 as 75 layers at 60 layers per inch. The MLI is double-aluminized Mylar (DAM) with double layer separators of B4A Dacron mesh. The 1/4-mil DAM weighs 8.788×10^{-3} kg/m^2 (1.8×10^{-3} lbm/ft^2), and the B4A Dacron weighs 6.347×10^{-3} kg/m^2 (1.3×10^{-3} lbm/ft^2). Blanket density is thus 5.0746×10^{-2} kg/m^3 (3.168 lb/ft^3), mounting components not included. It is anticipated that blanket weight will be a subordinate consideration in designing an alternate pressure control system.

The baseline CFME thermal analysis assumes the MLI effective thermal conductivity to be 2.08 W/m-k (1.2×10^{-5} Btu/hr-ft-R), per the following expression

$$k = 1.8824 \times 10^{-6} \, T_M^{0.6} \qquad (1)$$

in which T_M is the average blanket temperature in degrees Rankine. MLI studies of

References 2-3 and 2-4 recommend correlations yielding much lower conductivity values. However, Table VIII of Reference 2-5 tends to corroborate Equation 1 as quantitatively realistic. Following discussion with Mr. Pat Symons of NASA/LeRC, it was agreed that Equation 1 should be employed in this study.

Steady-state heat flux through the MLI blanket is presented in Figure 2-1 versus number of DAM layers over a range of hot side temperatures. Corresponding total heat rate through the MLI is similarly presented in Figure 2-2. The MLI blanket weight less attachment hardware is shown versus number of DAM layers in Figure 2-3. It will be shown that the equilibrium heat transport values of Figures 2-1 and 2-2 would not be realized in the initial 24 hours following CFME cooldown, and would only be approached asymptotically thereafter.

2.3 TRANSIENT ANALYSIS OF THE MLI BLANKET

The protracted transient thermal response of the MLI blanket must be taken into account in designing an alternate pressure control system. A nine-node transient analysis computer model was formulated for the numerical procedure of Reference 2-1. The model consisted of seven 0.508-cm (0.2-in) thick MLI nodes, set initially at 300K (540R) and bounded by inner and outer surface temperatures constrained at 22.2K (40R) and 300K (540R), respectively. This simulates an 84-layer blanket 3.56 cm (1.4 in) in thickness. The MLI thermal conductivity and density values noted in the previous section were employed, together with specific heat values ranging from 125.6 J/kg-K @ 22.2K, 732.7 J/kg-K @ 166.7K, and 1046.7 J/kg K @ 277.8K (0.03 Btu/lb-R @ 40R, 0.175 Btu/lb-R @ 300R, and 0.25 Btu/lb-R @ 500R).

Total heat rate through the MLI is presented in Figure 2-4 as a function of time after initiation of CFME cooldown. Thickness-direction temperature profiles at selected times during cooldown are presented in Figure 2-5. It is seen in both figures that equilibrium conditions are not yet achieved at 24 hours after tanking of the CFME. The heat rate schedule of Figure 2-4 provides the basis for succeeding thermal analyses of the CFME pressure vessel and tankage. Of interest in Figure 2-4, the initial heat rate exceeding 50 watts (170.7 Btu/hr) decreases to 16.4 watts (56 Btu/hr) at lockup, and decreases further to 7.18 watts (24.5 Btu/hr) at T-0.

2.4 TRANSIENT ANALYSIS OF THE FLAT-SURFACE MINIMUM ULLAGE CONDITION

Acceleration forces can be expected to maintain a flat surface ullage during the interval, lockup to SSME shutdown, a 4.13-hour duration. The thermal model of Figure 2-6 was employed to analyze the flat surface condition. Nodes 1 through 8 represent axisymmetric spherical segments of the pressure vessel wall. It will be seen in this, and later analyses, that heat conduction in the 0.142-cm (0.056-in) thick 6061 aluminum alloy wall is an important phenomenon to be exploited in designing a pressure control system for the CFME. Conductivity values of 167.88 W/m-K @ 17.5K and 202.49 W/m-K @ 24.7K (97 Btu/hr-ft-F @ 31.5R and 117 Btu/hr-ft-F @ 44.5R) were assigned

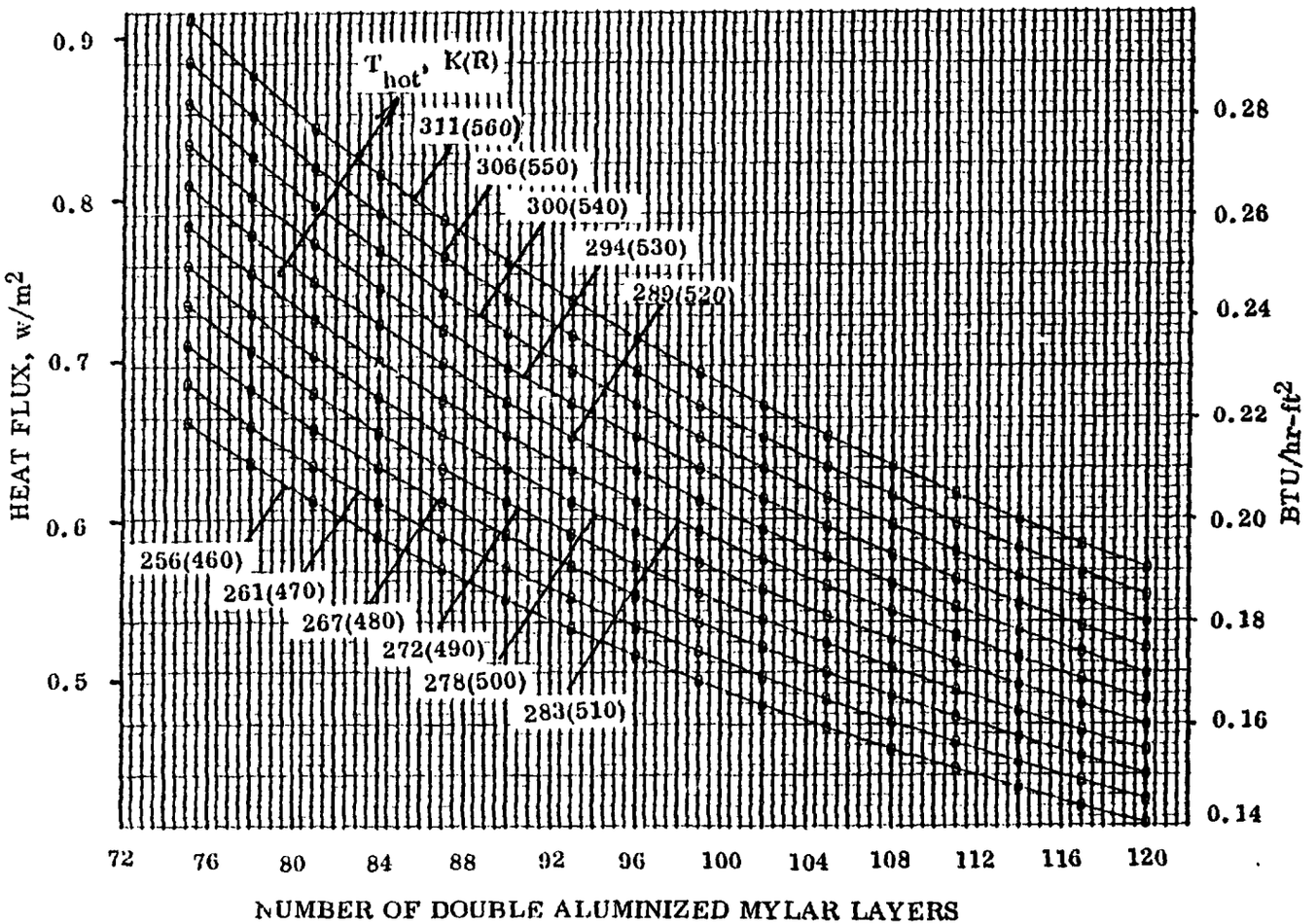

Figure 2-1. Installed Heat Flux Through CMFE Multilayer Insulation

ORIGINAL PAGE IS OF POOR QUALITY

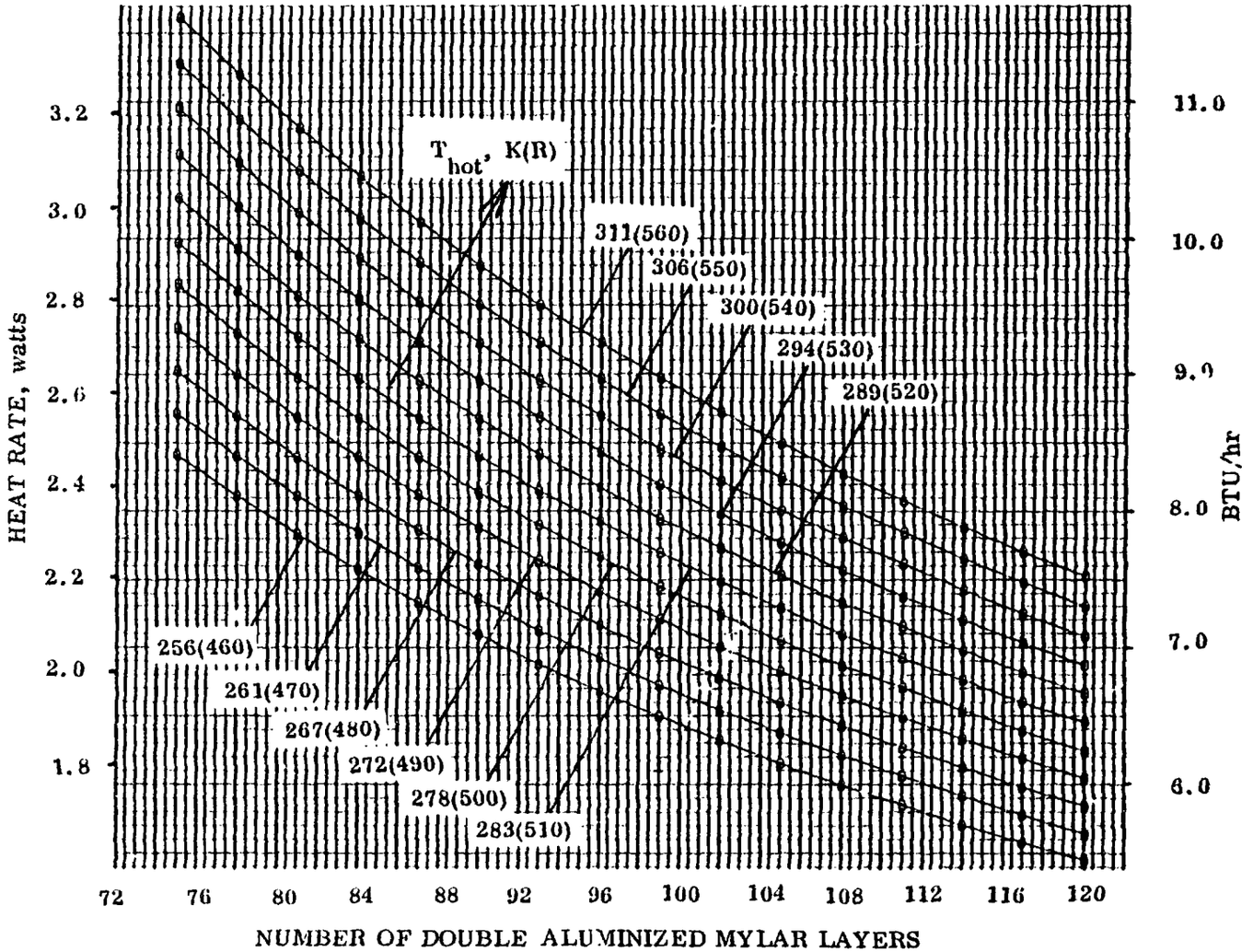

Figure 2-2. Installed Heat Rate Through CMFE Multilayer Insulation

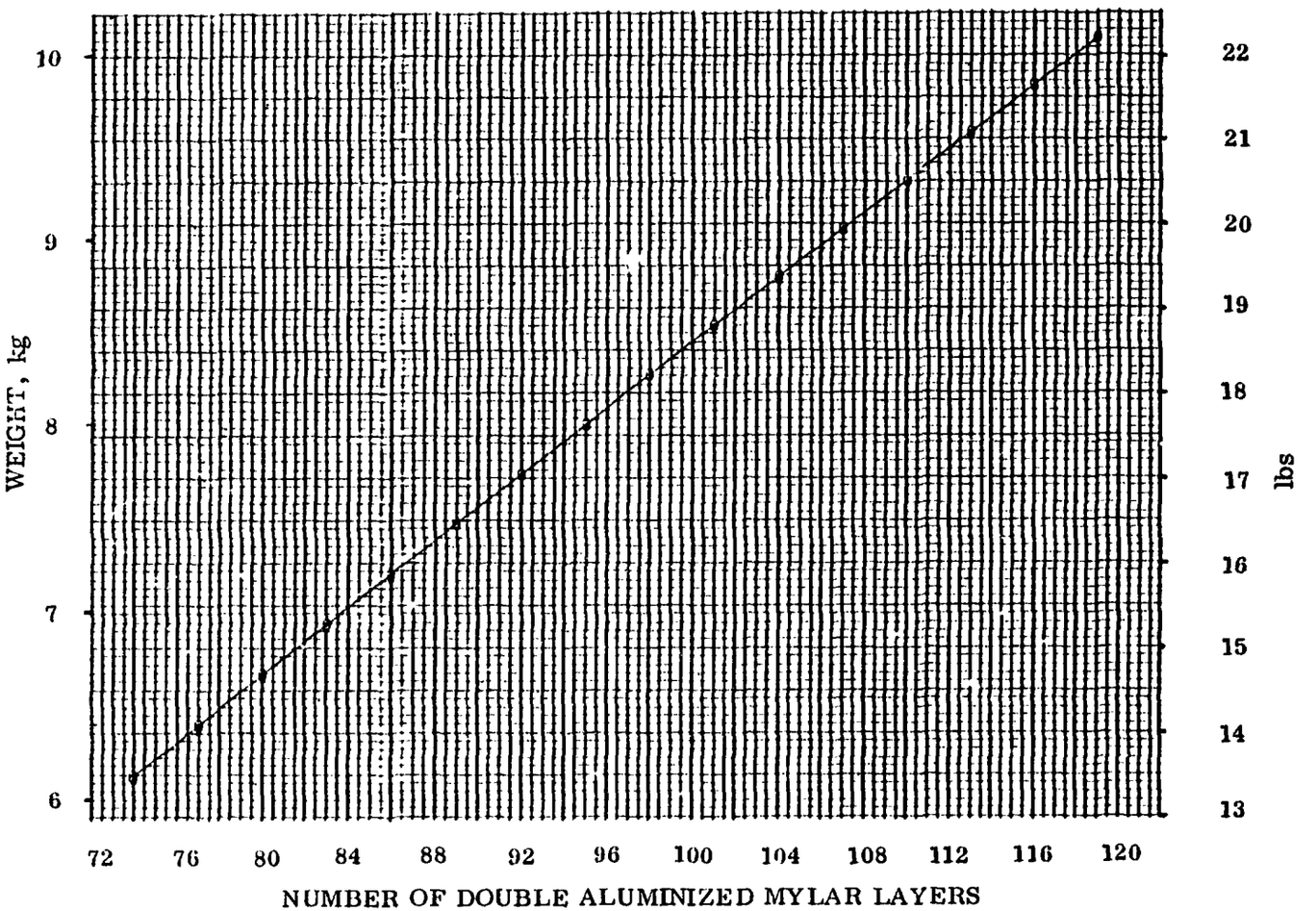

Figure 2-3. CFME Multilayer Insulation Weight Less Attach Fittings

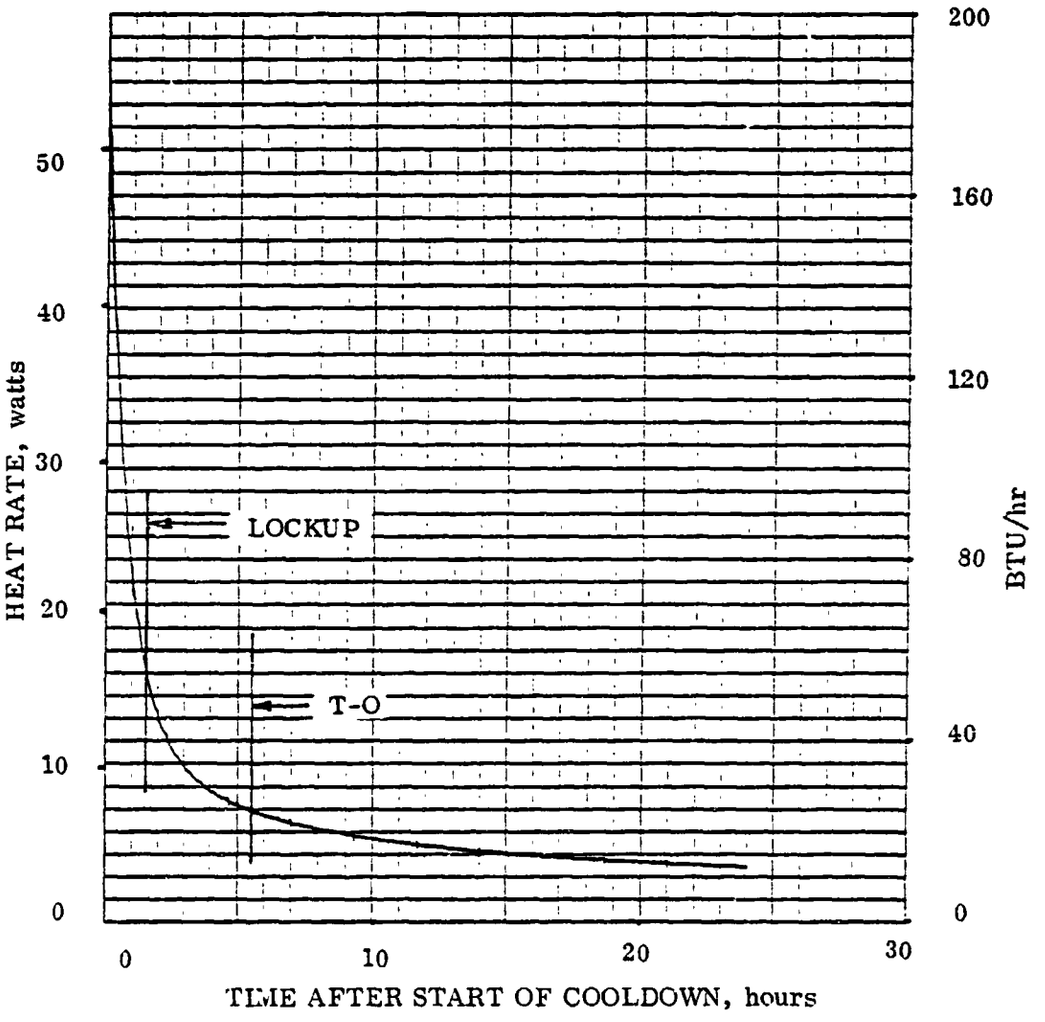

Figure 2-4. CFME Heat Rate Through MLI During Cooldown
(84 Layers DAM, 3.556 CM)

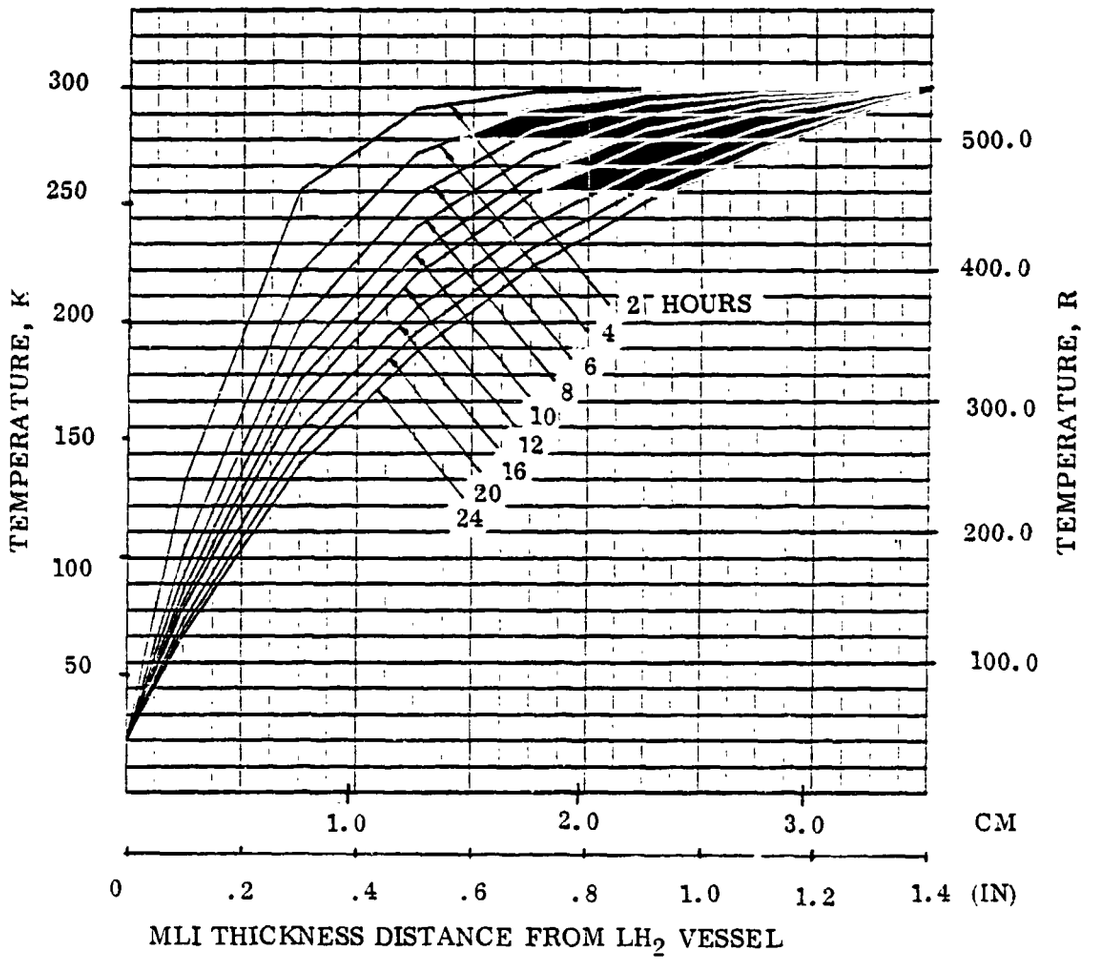

Figure 2-5. CFME MLI Temperature Profiles During Cooldown

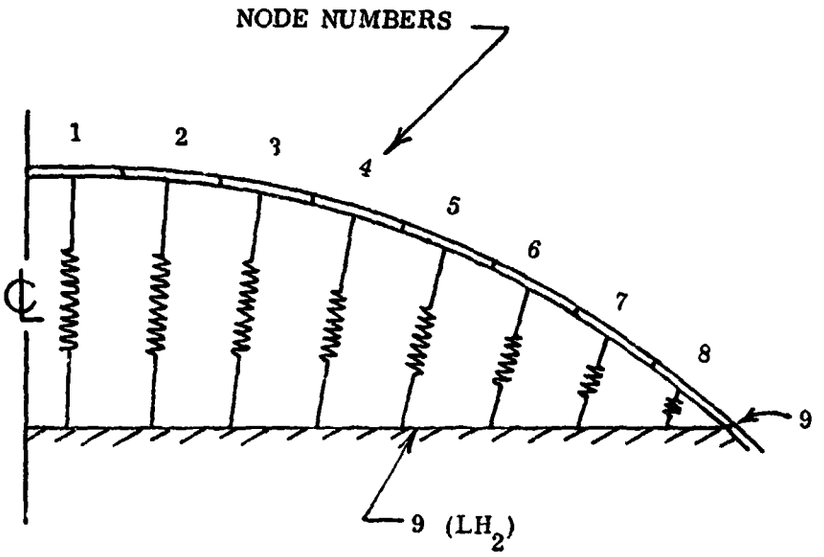

Figure 2-6. CFME Ullage Thermal Model, Lockup to SSME Shutdown

to the 6061 aluminum. Heat transfer in the ullage gas was conservatively assumed to be limited to the conductive mode. A heat flux schedule corresponding to the heat rate of Figure 2-4 between 1.5 and 5.5 hours was imposed on the surfaces of Nodes 1 through 8. Node 9, representing the LH_2, was arbitrarily increased from 21.3K (38.4R) to 22.2K (40R) over the 4-hour analysis interval.

Resulting temperature excursions of the pressure vessel wall nodes (Figure 2-6) are shown in Figure 2-7. It is seen that the warmest wall location (Node 1) warms rapidly to barely 0.6K (1.1R) above the liquid temperature, whereupon subsequent increases in all node temperatures are the result of the imposed temperature increase of the LH_2 (Node 9). Figure 2-8 contains the thermal mass-weighted average temperature of the unwetted wall as a function of time. Predicted net heat rate to the LH_2 is presented in Figure 2-9, also as a function of time.

2.5 TRANSIENT ANALYSIS OF THE ZERO-G MINIMUM ULLAGE CONDITION

The mutli-node analysis model of the zero-g minimum ullage condition is shown in Figure 2-10. It is seen that the simulation models the most unfavorable ullage location with respect to the location of pressure control heat exchanger number two (HX-2). The wedge-shaped analysis region is representative of a thermally axisymmetric CFME pressure vessel with 95 percent LH_2 in a zero-gravity environment. All nodes were modeled as rectangular paralleiepipeds, except for nodes 301, 302, 303 and 400. Node 400 was constrained to equal the thermal mass weighted average temperature of nodes 5, 15, 25, ··· 145, the LH_2 nodes bordering the ullage. Nodes 301, 302 and 303 are no-mass interface nodes, originally considered a possible location for HX-2. Heat conduction was assumed to be the only possible mode of heat transfer. The MLI heat rate of Figure 2-4 commencing at 5.63 hours (SSME shutdown) was expressed as a heat flux and imposed on the pressure vessel nodes.

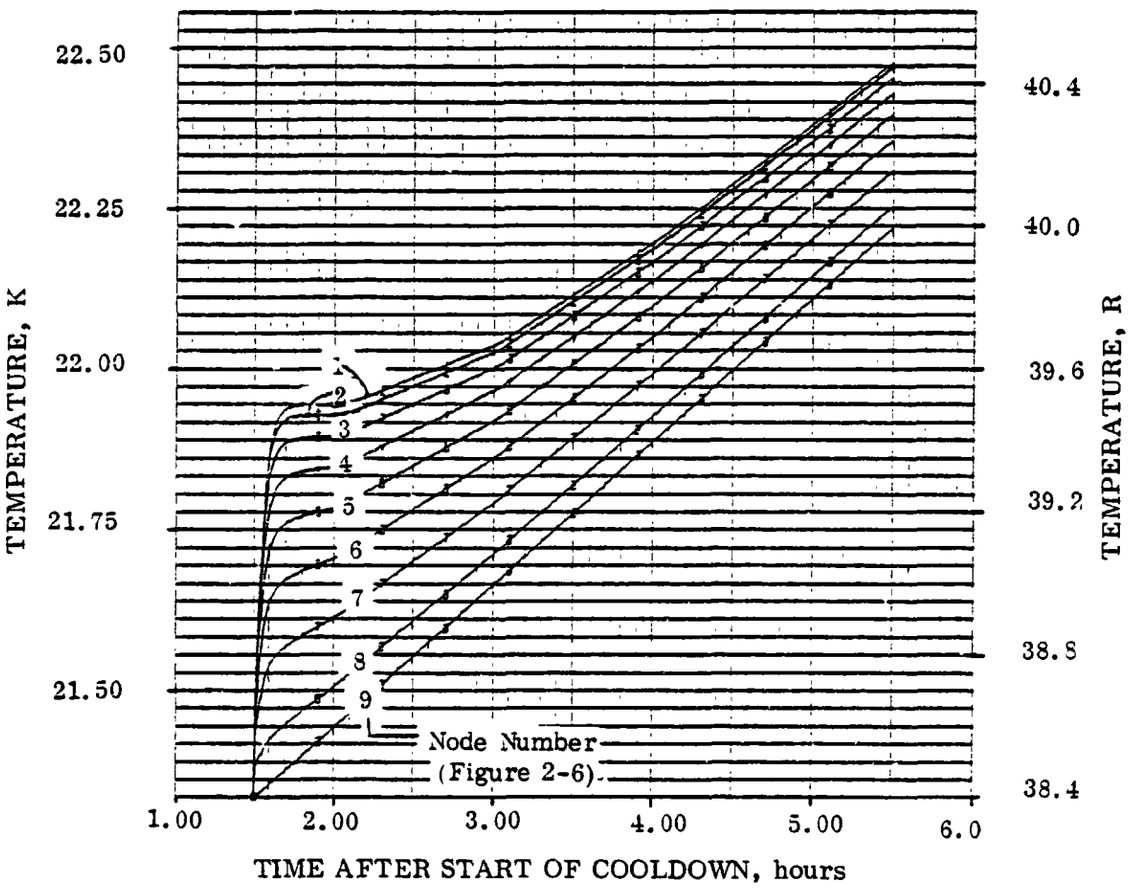

Figure 2-7. CFME Lockup Transient, Local Ullage Wall Temperatures

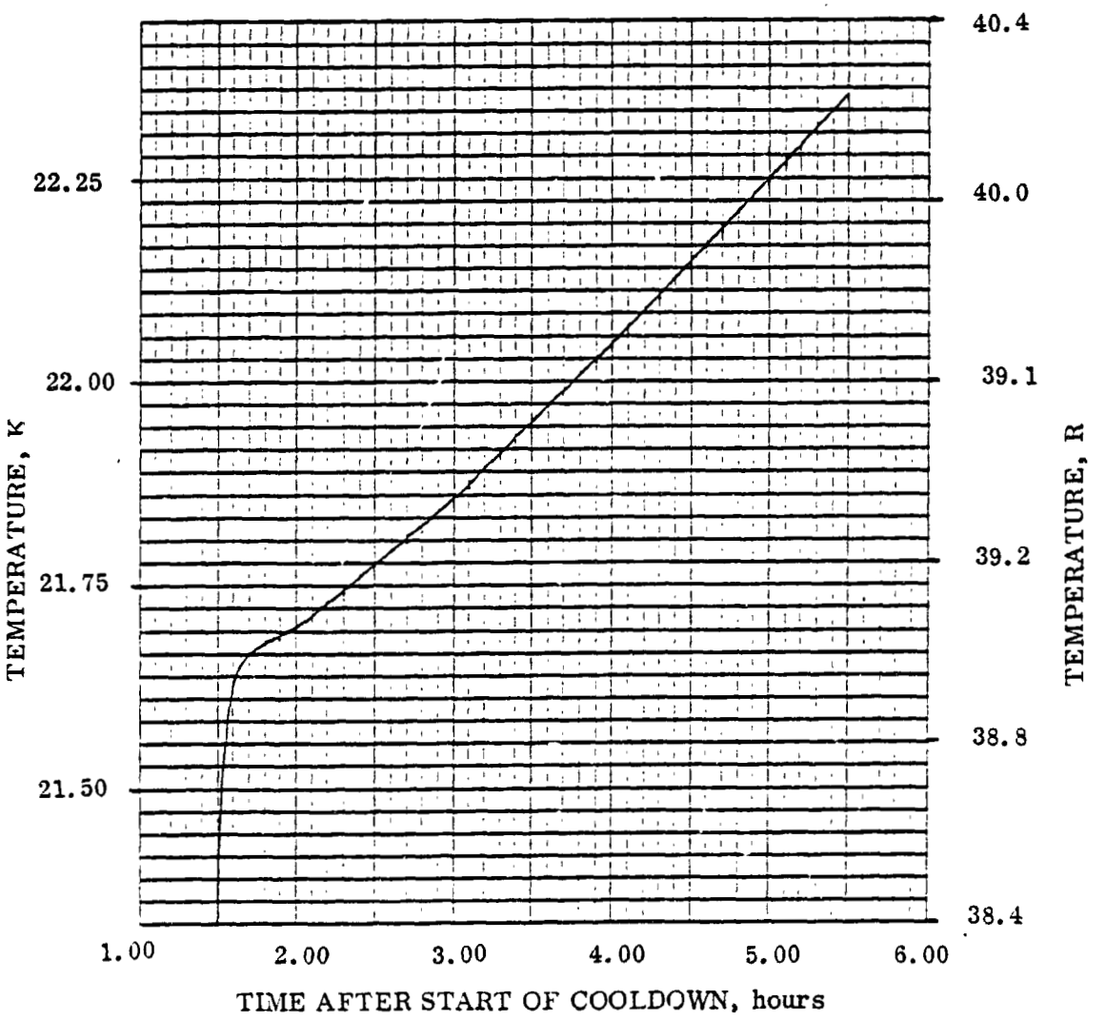

Figure 2-8. CFME Lockup Transient, Ullage Wall Mean Temperature

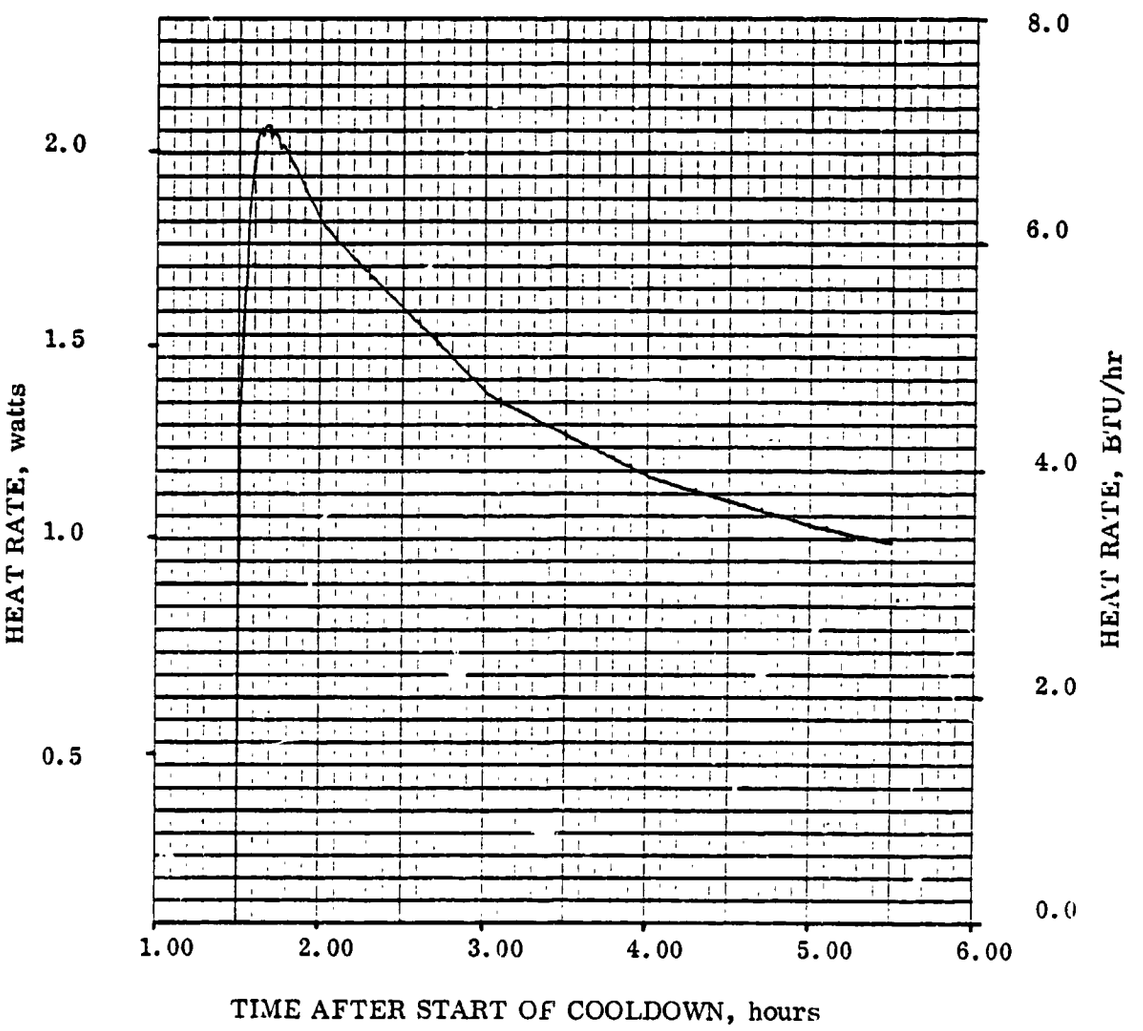

Figure 2-9. CFME Lockup Transient, Net Heat Rate to LH_2 Surface

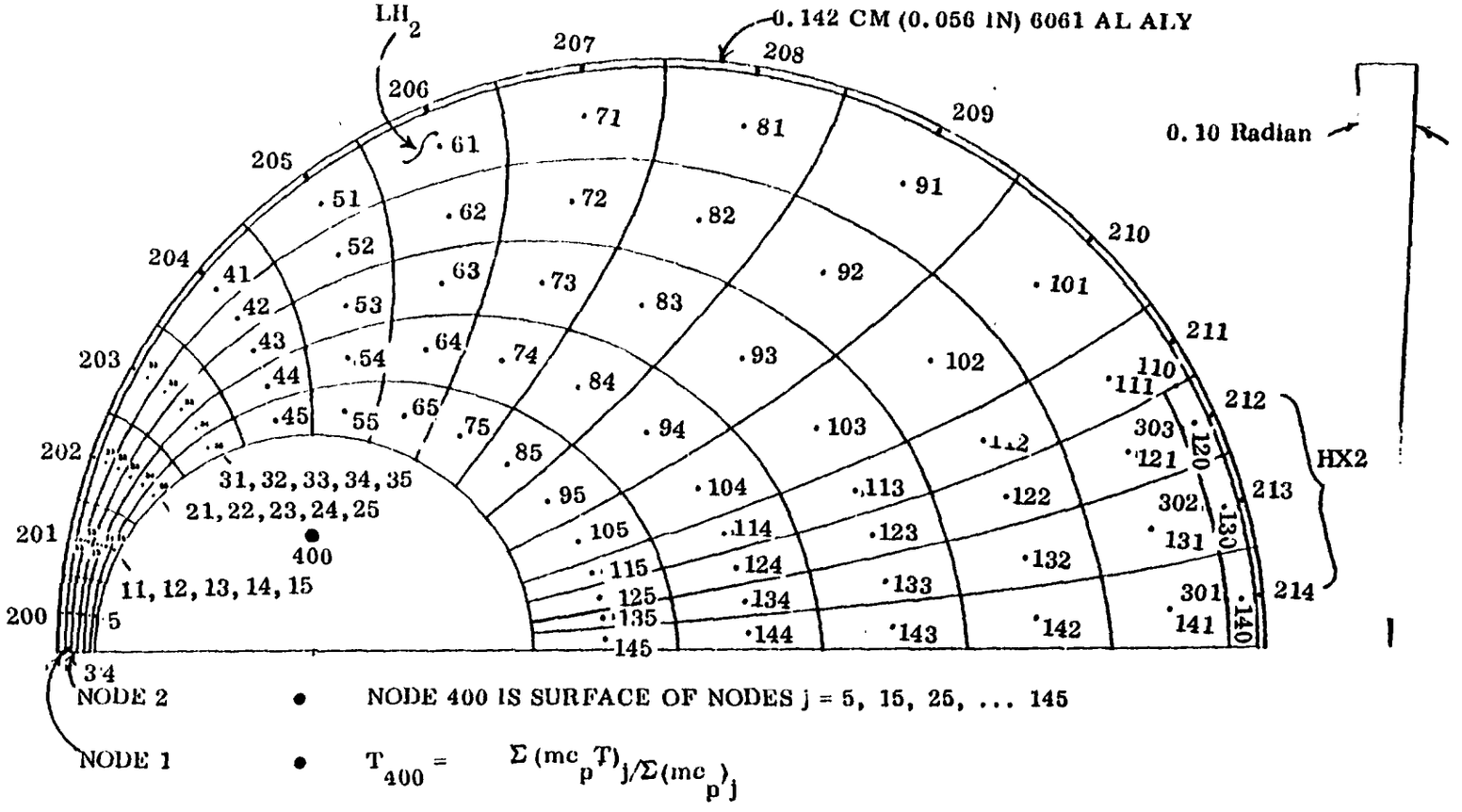

Figure 2 10. CFME Minimum-Ullage Thermal Model, Post-SSME-Shutdown

The temperature of Node 1 (see location in Figure 2-10) was employed as a thermostatic HX-2 control device. When Node 1 reached or exceeded 23.72K (42.7R), a heat extraction flux corresponding to 4.333 watts (14.79 Btu/hr), was imposed at HX-2, Nodes 212, 213 and 214. When a Node 1 temperature decrease reached 23.6K (42.48R) or less, HX2 heat extraction was interrupted.

Resulting temperatures are presented in Figure 2-11 as indicated by Node 1, in Figure 2-12 as indicated by Node 3, and in Figure 2-13 as indicated by the mean temperature of the ullage surface nodes (Node 400). It is seen in Figure 2-11 and 2-12 that HX-2 is activated at approximately 71 hours after CFME initial lockup. Ullage temperature control is seen to be responsive to HX-2 heat extraction, due to the high conductance of the pressure vessel wall. The latter effect is further demonstrated by the wall temperature profiles at the start and end of the first HX-2 cycle (Figure 2-14) and last HX-2 cycle (Figure 2-15), in which the HX-2 on times are 5 hours and 7.5 hours, respectively.

2.6 STEADY-STATE ANALYSIS OF THE ZERO-G MAXIMUM ULLAGE CONDITION

Analysis of the maximum ullage condition was performed on the basis of a preliminary assumption which placed HX-2 at the location of Nodes 301, 302 and 303 in Figure 2-10, 2.54 cm (1 in) inboard of the finally-adopted HX-2 location. HX-2 in its preliminary location was thus assumed to be linked to the adjacent pressure vessel wall by conduction through a 2.54 cm (1 in) layer of LH_2, a less efficient linkage than is obtainable by employing a metal-to-metal HX-2 installation.

The maximum ullage pressure vessel wall was assumed to be dry for a 78.2 cm (30.8 in) distance from HX-2, beyond which LH_2 @ 24.72K (44.5R) was assumed to reside (Figure 2-16). HX-2 was constrained at 20.83K (37.5R), and the ullage temperature was constrained at 24.72K (44.5R). A steady-state MLI heat flux of 0.788 W/m^2 (0.25 Btu/hr-ft^2) was imposed on the pressure vessel wall, and condensation heat transfer coefficients between the wall and the ullage of 1.362, 2.044 and 2.725 W/m^2 (0.24, 0.36 and 0.48 Btu/hr-ft^2-R) were imposed in separate cases. These condensation coefficients were obtained from Reference 2-6. They represent pessimistically low values based upon the presence of helium which serves to retard the molecular diffusion of vapor toward the condensing surface in a zero-g environment.

Resulting temperature profiles in the pressure vessel wall are shown in Figure 2-16. It is seen that HX-2 heat extraction from the vessel wall ranges from 2.980 W to 3.016 W (9.925 Btu/hr to 10.293 Btu/hr). Since the MLI heat rate to the dry wall is only 1.865 W (6.365 Btu/hr), the net ullage-to-wall heat extraction is 1.043 to 1.151 W (3.56 to 3.928 Btu/hr). The closely similar wall temperature profiles show that HX-2 performance would not be adversely affected by a large variation in ullage-to-wall heat transfer coefficient.

2.7 HX-2 THERMAL DESIGN ANALYSIS

HX-2 must consist of a coil of small diameter (approximately 0.47625 cm (0.1875 in) 6061 Al Aly tubing affixed to the pressure vessel wall over an area of approximately 0.186

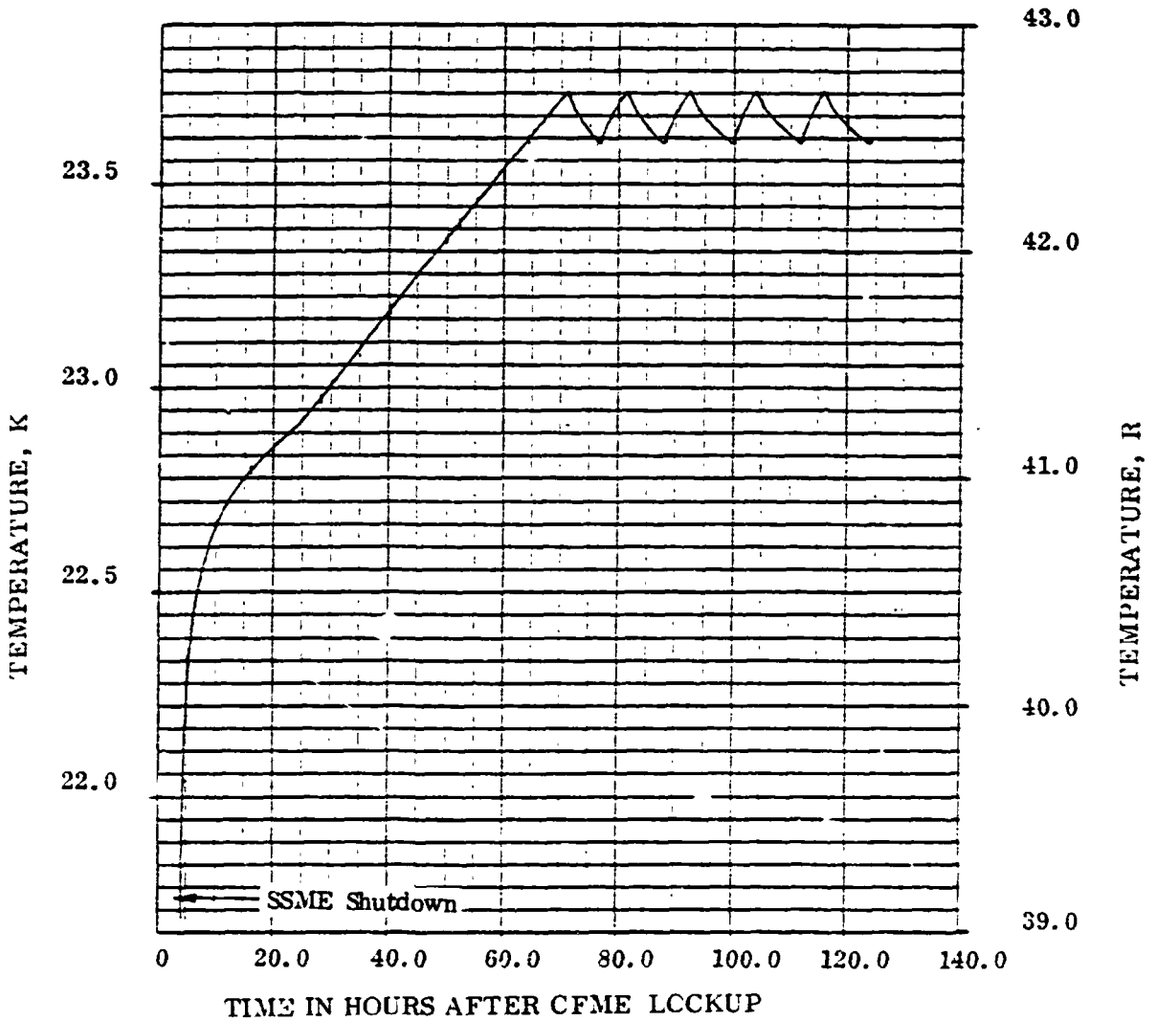

Figure 2-11. CFME Liquid Temperature as Indicated by Node 1, No Convection, 4.333 Watts (14.79 Btu/Hr) HX-2 Heat Extraction

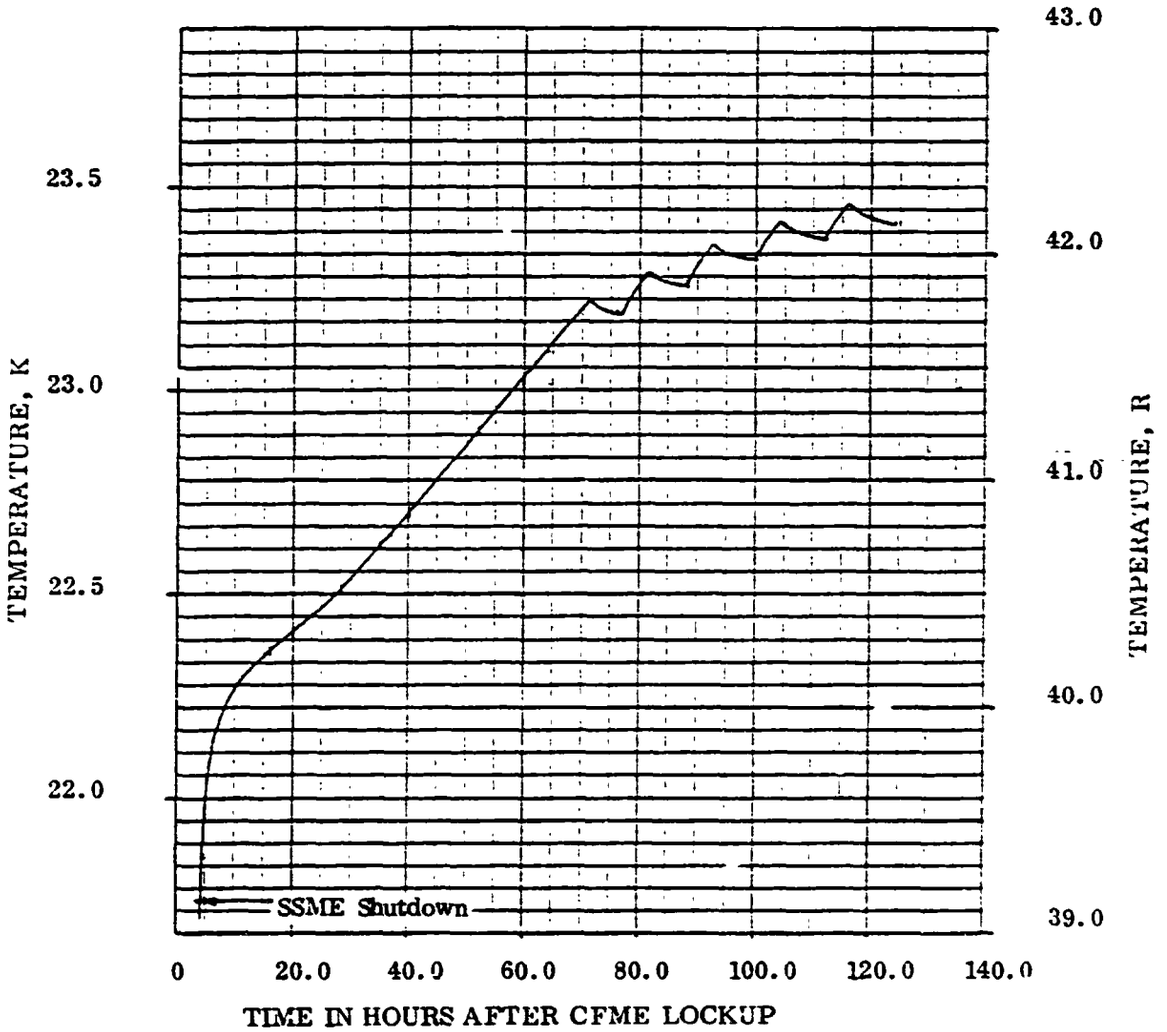

Figure 2-12. CFME Liquid Temperature as Indicated by Node 3, No Convection, 4.333 Watts (14.79 Btu/Hr) HX-2 Heat Extraction

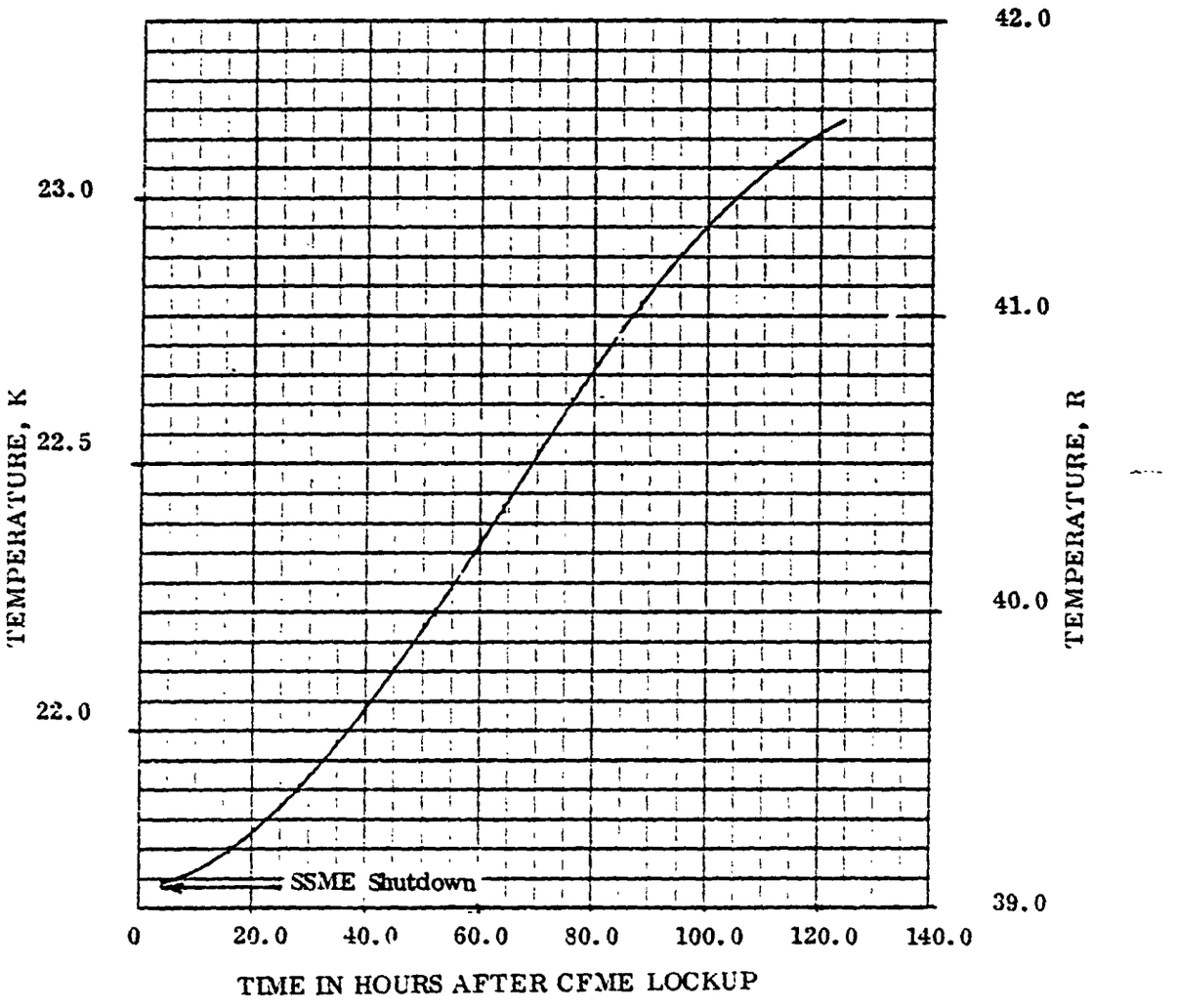

Figure 2-13. CFME Ullage Surface Nodes Mean Temperature, No Convection, 4.333 Watts (14.79 Btu/Hr) HX-2 Heat Extraction

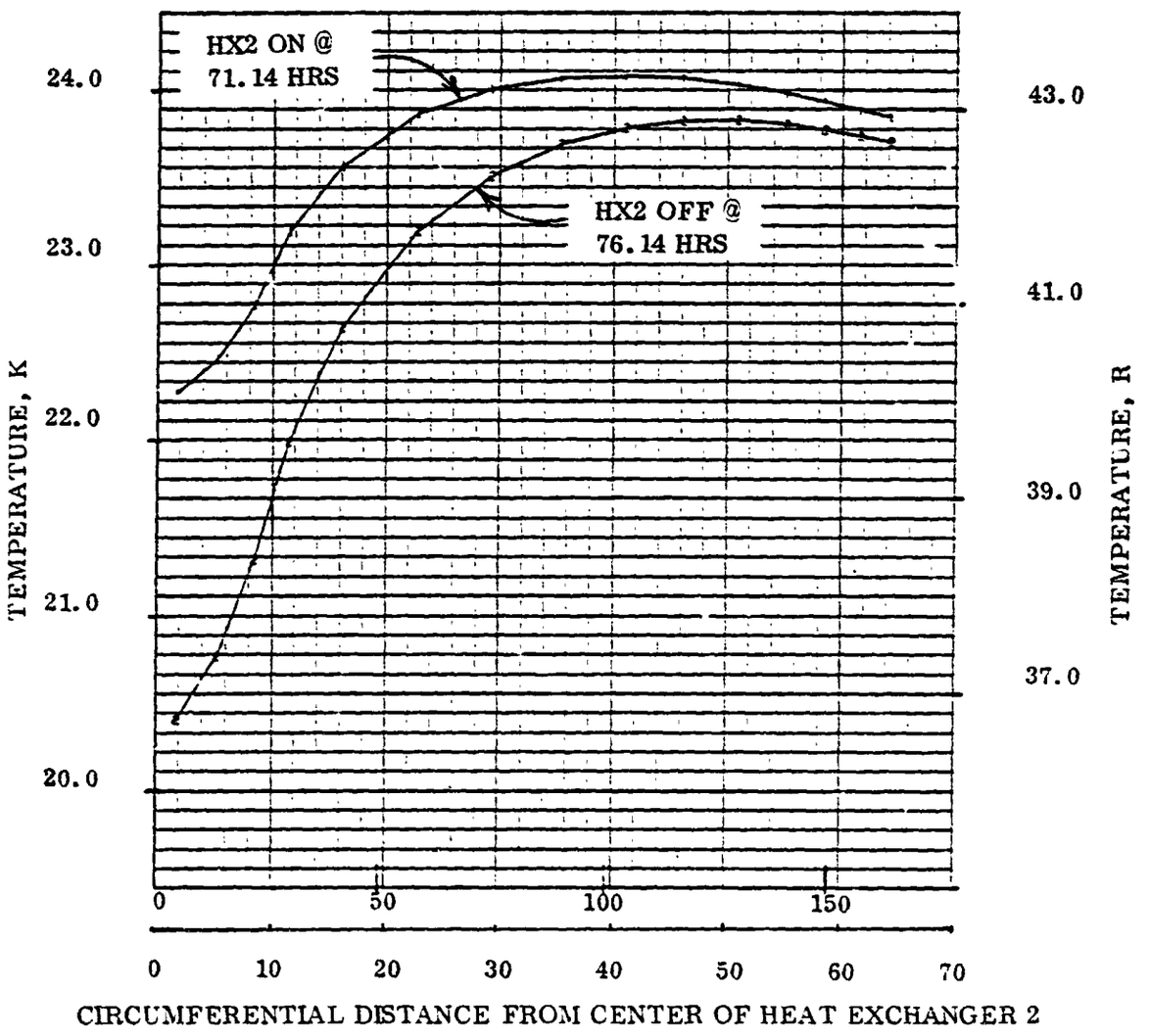

Figure 2-14. CFME Pressure Vessel Temperature Profile at Start and End of First HX-2 Cycle

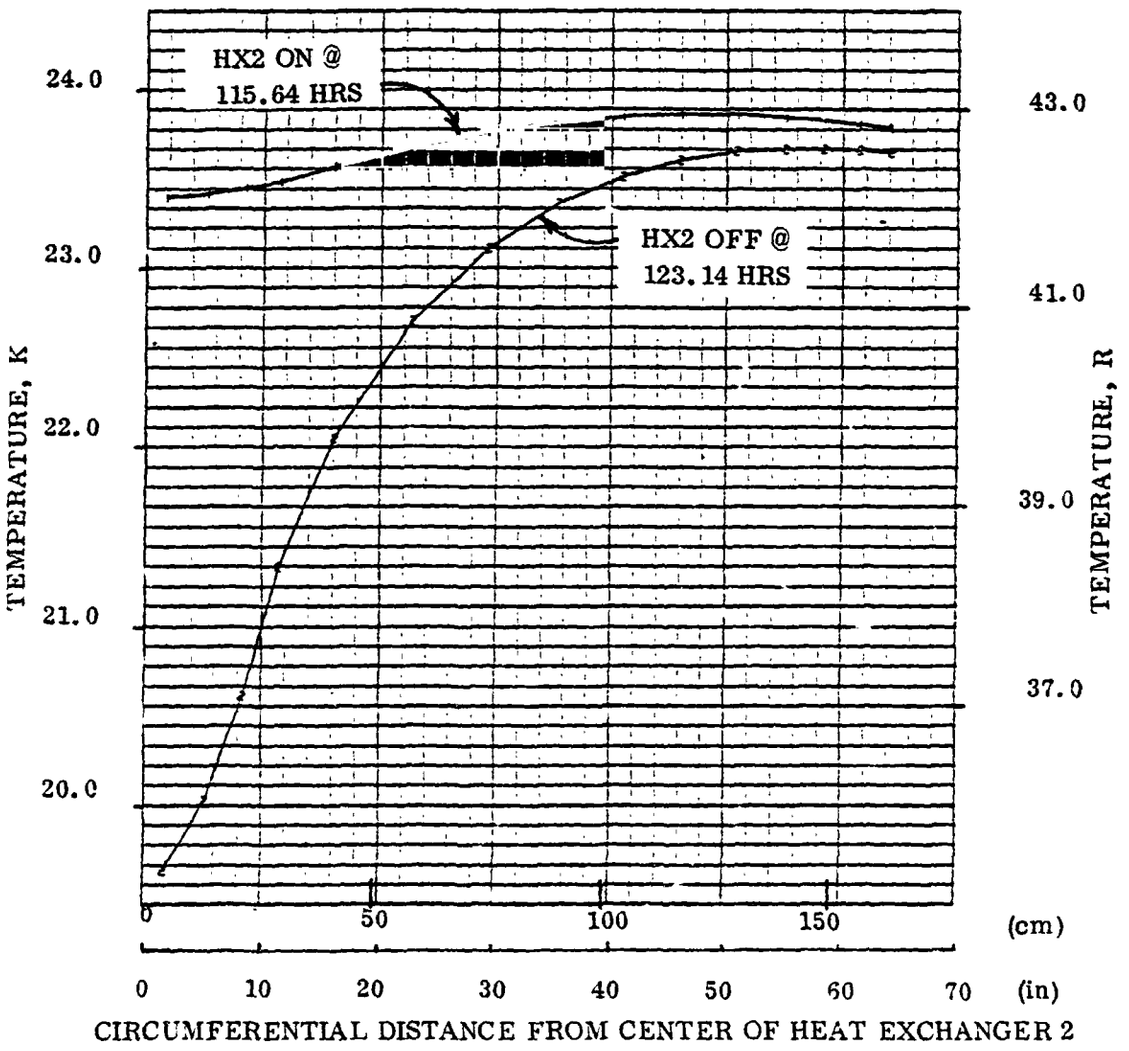

Figure 2-15. CFME Pressure Vessel Temperature Profile at Start and End of Last HX-2 Cycle

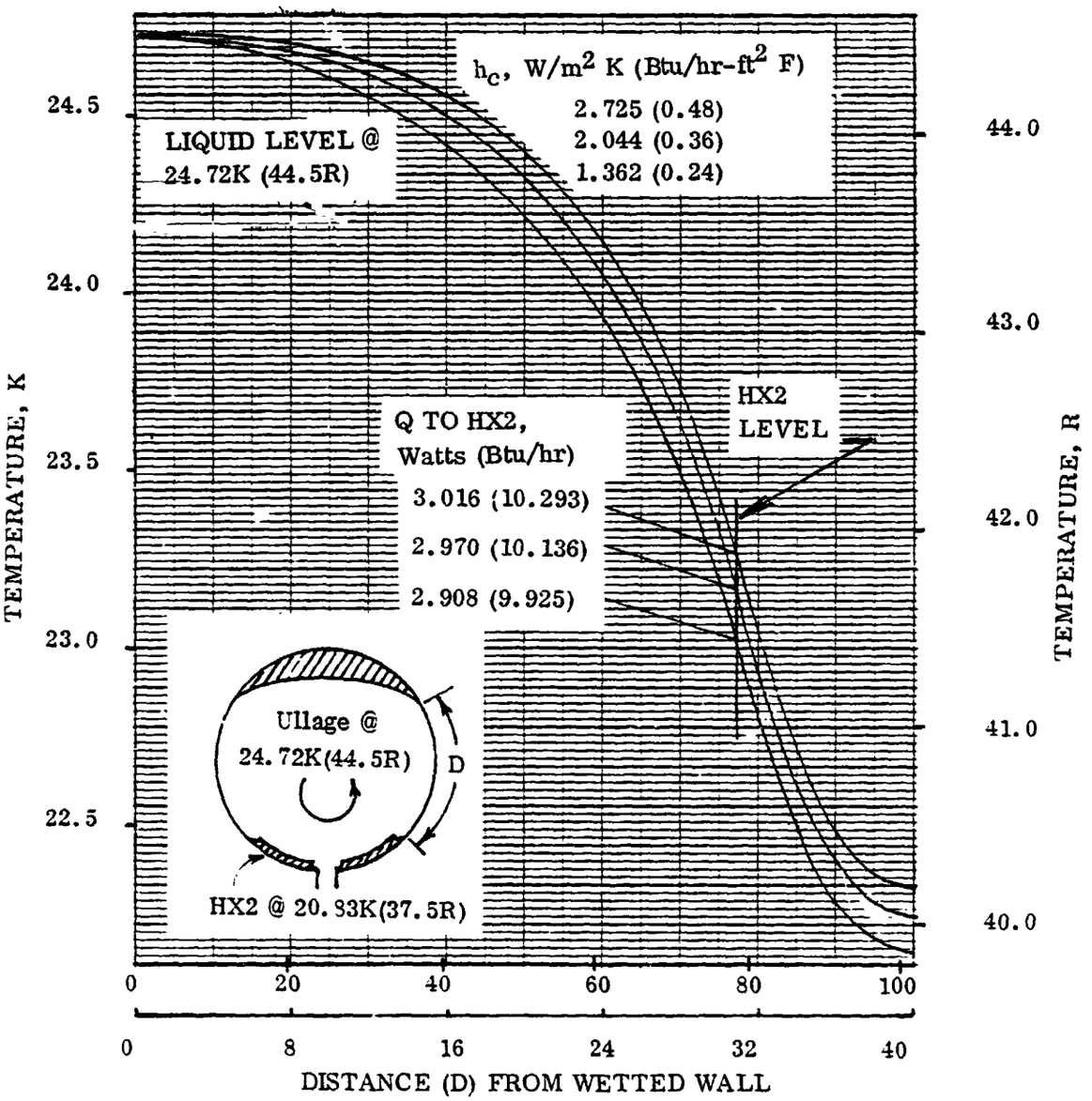

Figure 2-16. CFME Pressure Vessel Temperature Profiles With Maximum Ullage and Various Condensation Heat Transfer Coefficients

m^2 (2 ft^2) around the vessel outlet. The tubing must either be dip-brazed to the pressure vessel wall, or to a 6061 Al Aly plate which in turn, must be welded at its edges to the pressure vessel. The latter fixture must comprise a continuously-conductive path in 6061 Al Aly, as reflected in the previous thermal analyses. Figure 2-17 contains a sketch of the proposed heat exchanger installation. The following analyses will quantify an appropriate spacing between adjacent tubing coils, and will define HX-2 area and tubing length.

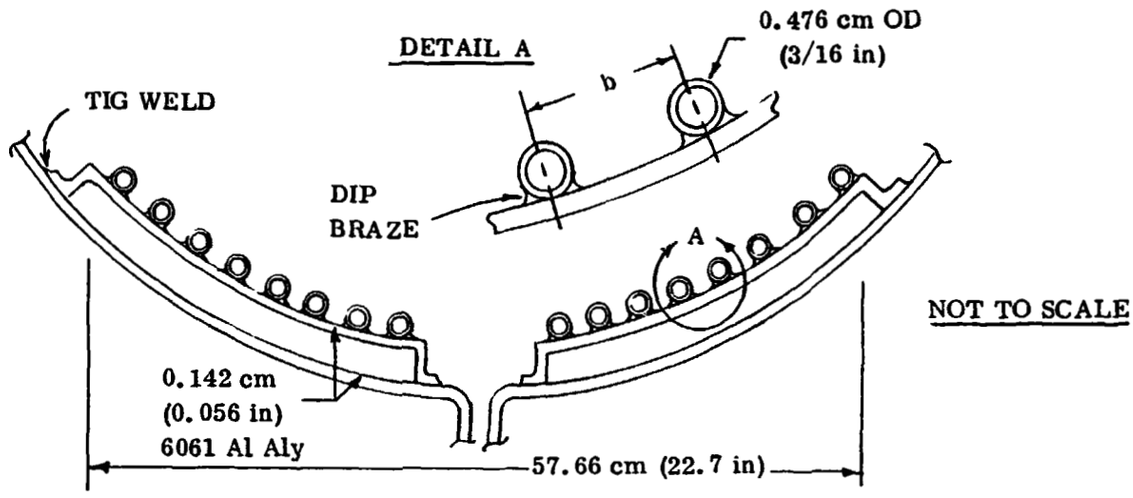

Item	Analysis	Final Design
HX2 Area, m^2 (ft^2)	0.173 (1.858)	0.211 (2.267)
Tube Spacing b, cm (in)	2.54 (1.0)	2.54 (1.0)
Tube Length, m (ft)	6.6 (21.67)	10.21 (33.50)

Figure 2-17. Alternate HX2 Installation Concept

2.7.1 HX-2 COIL SPACING. Let it be assumed that HX-2 covers an area, A_{HX} of 0.173 m^2 (267.6 in^2) to which is affixed coiled tubing, continuously soldered. Assume the tubing coils reside at spacing b. Assume q to be a uniform heat flux extracted from the liquid

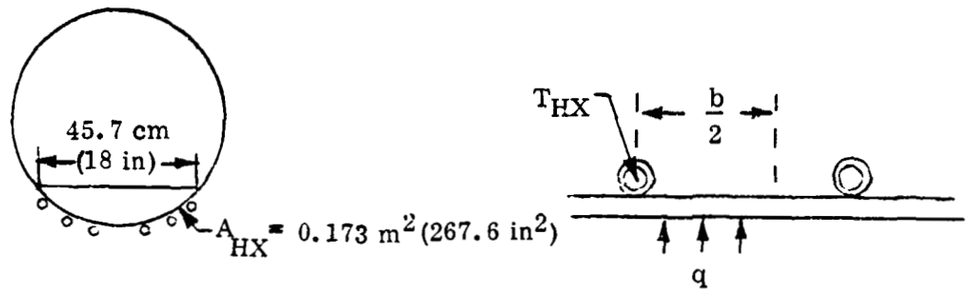

when the HX-2 liquid boils at T_{HX}, and

$$Q = q\,A_{HX}$$

$$D = T - T_{HX}$$

The ordinary differential equation

$$\frac{d}{dx}\left(-kA\frac{dD}{dx}\right)dx = q\,dx \tag{2}$$

reduces to

$$\frac{d_2D}{dx^2} + \frac{q}{kA} = 0 \tag{3}$$

in which A is the cross-sectional area for conduction. The general solution of (2) is

$$D + \frac{qx^2}{2kA} + C_1x + C_2 = 0 \tag{4}$$

and the appropriate boundary conditions are

$$\frac{dD}{dx} = 0 \;@\; x = \frac{b}{2}$$

$$D = 0 \;@\; x = 0$$

The particular solution is

$$D = \frac{qx}{2kA}(b-x) \tag{5}$$

It is of interest to note that the heat conduction to T_{HX} must equal Q. If tubing length is L

$$L = \frac{A_{HX}}{b}$$

$$Q = 2LkA\left(\frac{dD}{dx}\right)_{x=0} \tag{6}$$

Differentiation of (5) for x = 0 and substitution of A_{HX}/b for L yields from (6)

$$Q = q\, A_{HX}$$

D_{max} at x = b/2 is

$$D_{max} = \frac{qb^2}{8kA} \tag{7}$$

$\bar{D}$, the mean wall temperature is

$$\bar{D} = \frac{2}{b} \int_0^{b/2} D\, dx \tag{8}$$

Substitution of (5) in (8) and integration yields

$$\bar{D} = \frac{qb^2}{12\, kA} \tag{9}$$

and comparison of (7) and (9) shows that the temperature profile between tubes is a typical parabola

$$\bar{D}/D_{max} = 2/3$$

Substitution in (9) of k = 178.3 W/m-K (103 Btu/hr-ft-R), $A = 4.335 \times 10^{-4}\ m^2$ ($0.056/12\ ft^2$), b = 0.0254 m (1/12 ft), and Q = 5.86W (20 Btu/hr), for which $q = Q/A_{HX}$, yields the following interesting result: $\bar{D} = \bar{T} - T_{HX} = 0.0072K$ (0.013R).

It is thus seen that the highly conductive pressure vessel wall cannot sustain a temperature gradient for Q = 5.86W (20 Btu/hr) and a tube spacing of b = 2.54 cm (1 in). It is therefore tentatively concluded that approximately 6.6m(260 in) of tubing with a 2.54 cm (1 in) spacing between coils will yield a strongly conservative design for HX-2 because Figures 2-14 and 2-15 show a wall temperature near 20.56K (37R) at the HX-2 location. Heat extraction would thus not be penalized by conductive resistance in the HX-2 attachment, but would be limited at all times by ventage flow rate.

2.7.2 HX-2 AREA AND TUBING LENGTH

Since HX-2 heat extraction will be a pure function of ventage temperature and flow rate, rigid dimensional requirements for HX-2 need not prevail. It will be seen in Section 4.1.1 that an inner coil radius of approximately 10 cm (4 in) is a practical requirement to permit welding of the HX-2 plate sections to the pressure vessel. Let it therefore be assumed that the tubing is arranged in eight (8) coils with a 2.54 cm (1 in) spacing between coils. The coil shape is a classical spiral of Archimedes

$$\rho = \frac{\theta}{2\pi} + 10 \qquad (10)$$

and $\theta = 16\ \pi$ for eight coils. Tubing length, L, is calculated by conventional integration.

$$L = \int_0^{\theta} \left[\rho^2 + (d\rho/d\theta)^2 \right]^{1/2} d\theta \qquad (11)$$

Resulting length of tubing from (10) and (11) is 10.216 m (33.52 ft). To accommodate eight coils, the plate will cover a wall area of 0.284 m^2 (3.057 ft^2). However, as will be seen in Section 4, the plate must be interrupted in four locations at which the CFME acquisition device is installed. Net HX-2 area will thus be 0.211 m^2 (2.267 ft^2). Tubing length and plate area thus exceed the corresponding values employed in the analysis of 2.7.1, further assuring complete vaporization of the HX-2 ventage.

2.8 THERMAL ANALYSIS CONCLUSIONS

1. Parametric thermal analyses of the CFME MLI blanket over a range of thicknesses and hot side temperatures have yielded steady-state heat rate data and MLI weight data, permitting blanket optimization (Figures 2-1 through 2-3).

2. Transient analysis of an 84-layer, 3.556 cm (1.4 in) DAM MLI blanket has yielded a schedule of MLI heat rate versus time after initial cooldown, together with thickness-direction MLI temperature profiles (Figures 2-4 and 2-5).

3. The transient heat rate data of Figure 2-4 have been employed as input to analysis of a flat surface minimum ullage condition. The transient analysis covers the interval, CFME lockup to SSME shutdown. Resulting data (Figures 2-7 through 2-9) provide the basis for prediction of ullage pressure response during flat-surface ullage conditions.

4. A detailed transient thermal analysis of the zero-g minimum ullage condition has demonstrated the effect of 4.333 W (14.79 Btu/hr) HX-2 heat extraction as a method of limiting ullage temperature. Thermal response predictions (Figures 2-11 through 2-15) provide the basis for post-SSME shutdown pressure predictions.

5. A steady-state analysis of the zero-g maximum ullage condition shows that HX-2 heat extraction values less than the 4.333 W (14.79 Btu/hr) design value can still control (maximum) ullage temperatures (Figure 2-16).

6. HX-2 tubing coil spacing and plate area analyses have yielded a recommended tubing length of 10.216 m (33.52 ft), a 2.54 cm (1 in) coil spacing, and an HX-2 plate area of 0.211 m^2 (2.267 ft^2).

7. The CFME alternate pressure control thermal analyses have demonstrated the importance of the highly-conductive pressure vessel wall. This feature of the pressure vessel has accordingly been exploited in the alternate system design approach.

3

ALTERNATE PRESSURE CONTROL SYSTEM THERMODYNAMIC ANALYSIS

Analyses were conducted in this area to determine how CFME tank pressure control and vent mass would be affected by the predicted heating environment to the alternate CFME configurations. Tank pressure control is of concern for these configurations because heat flow through the MLI will be absorbed by the propellant. Consequently, a higher tank pressure rise rate will result unless HX-2 (for each configuration) is designed to remove energy from propellant at a rate equivalent to that removed by the VCS.

A thermodynamic analysis was performed comparing CFME pressures and mission vent mass requirements of the baseline to the alternate configurations. An analysis of Concept No. 1 was performed to determine its pressure control capability. A similar analysis could not be performed on the baseline configuration because of insufficient performance data. However, thermal equilibrium analyses were conducted which permitted an evaluation of the VCS advantages and disadvantages.

3.1 ASSESSMENT OF TVS ALTERNATES

One of the first tasks performed in this study was a comparative thermodynamic assessment of the alternate TVS configurations. This work was performed to identify major advantages or disadvantage of each system in order to focus on the key issues. This assessment is summarized in Figure 3-1; Alternate Concept No. 2 was found to be deficient to the point of terminating further analysis.

3.1.1 BASELINE CFME. TVS operation was discussed in Section 1.1.2. Basically, liquid propellant is withdrawn from the CFME and flows through HX-1 and HX-2, intercepting heat penetrations as well as radiation heat transfer to the VCS. The presence of the VCS allows GH_2 to exit HX-1 at temperatures as high as 93.3K (165R) Vent flowrate at this exit temperature can be determined from Figure 3-2 and is given in Table 3-1. It is evident from Figure 3-2 that reduced vent mass requirements occur as vent gas temperatures are increased. Thus, high vent gas temperatures will provide high thermal performance for HX-1 and HX-2 as well.

HX-2 appears to have conflicting performance requirements. First, there is the need to achieve and maintain the high thermal performance made possible by the VCS, i.e., operate HX-2 to vent a high temperature vapor. There is also the requirement for propellant tank pressure control which is the primary function of HX-2. Tank pressure control will occur when net heating to the pressure vessel is reduced to zero or becomes negative, which is possible only if there is heat transfer to a low temperature vent gas.

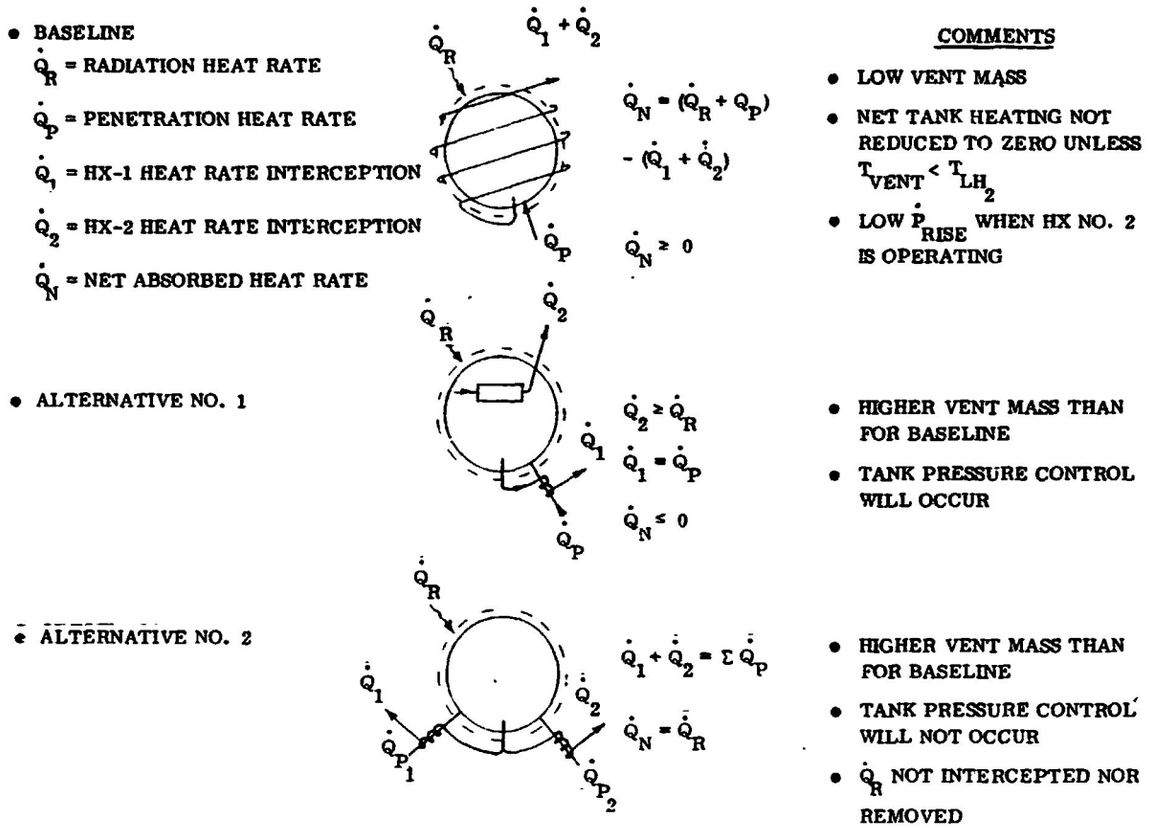

Figure 3-1. Thermodynamic Assessment of Alternate Concepts

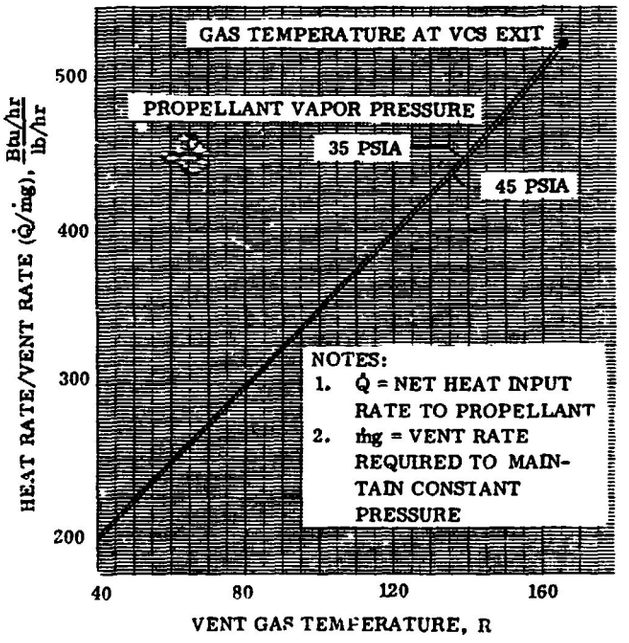

ORIGINAL PAGE IS OF POOR QUALITY

Figure 3-2. Requirements for Constant Pressure Venting of CFME Propellant Vessel

Table 3-1. Comparison of Alternative CFME Heat Exchanger Design Conditions

Configurations	Heat Extraction, watts (Btu/hr)		Vent Rate[1]	
	Steady-State	Design	kg/hr	(lb/hr)
Baseline[2]				
HX-1 (Continuous Vent Flow)	4.76 (16.24)	4.76 (16.24)	0.0141	(0.0311)
HX-2 (Pressure Controlled)	2.37 (8.10)	3.56 (12.15)[3]	0.0105	(0.0232)
Alternate No. 1				
HX-1 (Continuous Vent Flow)	4.17 (14.24)[4]	4.17 (14.24)	0.0323	(0.0712)
HX-2 (Pressure Controlled)	2.89 (9.86)[4]	4.33 (14.79)[3]	0.0335	(0.0740)

1. Obtained from design heat rate extraction and Figure 3-2.
2. Heating rates were a study groundrule (Table 1-1).
3. Sized for 150 percent of heat extraction rate.
4. Steady-state heat rate selected to extract penetration heat rates identified by Table 1-1. Steady-state heat rate is based upon an 84-layer MLI blanket.

If both requirements cannot be satisfied high thermal performance will have to be sacrificed since satisfactory pressure control is mandatory.

Since there was insufficient data available to properly assess the thermal performance and pressure control capability of HX-2, it became necessary to make an assumption regarding thermal control, and to employ engineering judgment regarding pressure control. For the comparative assessment, vent gas temperature was selected to be the same for HX-2 as for HX-1. This should favor the baseline CFME configuration. A judgment was made regarding the ability of HX-2 to control vessel pressure. It was concluded that although satisfactory pressure control would occur, it was felt that the ability to reduce tank pressure could substantially reduce HX-1 and HX-2 thermal performance during the tank pressure-control period.

3.1.2 ALTERNATIVE NO. 1. This configuration is identical to the baseline with the following exceptions:

1. The vapor-cooled shield is deleted.

2. HX-1 is selected to intercept all conduction heating penetrations, and is assumed to be equal in weight to the baseline HX-1.

3. HX-2 is mounted to the inside walls of the pressure vessel (Figure 2-17). This HX will control tank pressure by extracting energy directly from the propellant.

VCS removal will result in a lower thermal performance for this configuration since the VCS provides additional capability for heat absorption by the vent fluid. A vent gas temperature of 22.2K (40R) was selected for current HX-1 and HX-2 operation, which is lower than liquid temperature. This is a pessimistic assumption because a vent temperature higher than liquid temperature should not be difficult to achieve.

It is evident that thermal performance for this concept will be poorer than for the baseline configuration. Figure 3-2 indicates that vent flowrate requirements will be about 250 percent greater (for constant pressure venting) than for the baseline configuration. Vent flowrate requirements for HX-1 and HX-2 operation are given in Table 3-1

The tank pressure control capability of an internal tank heat exchanger (HX-2) is potentially greater than for the baseline configuration, primarily due to the close thermal contact between heat exchanger and the tank fluid required for energy extraction. On the other hand, the baseline TVS (with VCS) is designed to intercept heat before it is absorbed by the propellants. This latter design approach inherently isolates HX-2 from the tank propellants. Another advantage for the alternate concept is that it can be designed for a higher vent flowrate to improve tank pressure control capability. This can be achieved without impacting thermal performance. Conversely, thermal performance for the baseline configuration is degraded as vent flowrate increases.

There is the task of predicting CFME pressure response to HX-2 operation, which is addressed in Section 3.2.

3.1.3 ALTERNATE NO. 2. A study groundrule for this configuration was that both HX-1 and HX-2 must be mounted external to the CFME vessel. It was further stipulated that HX-2 could not be mounted to the outside walls of the vessel. These restrictions eliminated the possibility of excellent thermal contact between HX-2 and the tank propellant. Consequently, HX-2 was restricted to an operating mode virtually identical to that of HX-1, namely intercepting heating penetrations. The only capability for propellant energy extraction would be by conducting energy along the existing penetrations to the low temperature vent fluid. It did not appear likely that the steady-state radiation heat rate to the propellants of about 2.9 watts (10 Btu/hr) could be effectively removed in this manner. Thus it was concluded that alternate No. 2 would not be capable of tank pressure control. Because of this serious deficiency, alternate No. 2 was eliminated from further consideration.

3.2 THERMAL EQUILIBRIUM ASSESSMENT

CFME pressure history and vent mass requirements during the seven-day mission will depend upon how the heat input is distributed to the tank fluid. The ideal situation would be for thermal equilibrium conditions to exist throughout the mission. Thermal equilibrium occurs when liquid and vapor are at the same temperature. This condition guarantees that pressure rise rates are minimized for a given heat input rate. Thermal

equilibrium conditions will also minimize vent mass requirements for the CFME mission.

It is expected that the following factors will tend to provide near-equilibrium fluid conditions for the CFME mission: (1) a low heat input rate, (2) g-jitter, and (3) the high thermal conductivity of the aluminum vessel.

The low heat input rate provided by the MLI blanket will result in a lower temperature gradient in the liquid and vapor phases to support the low heat exchange rates.

G-jitter refers to transient perturbations to the gravity field that can arise from vehicle maneuvers and mechanical vibrations. It is possible that disturbances as large as 10^{-3} g may occur during the CFME mission. This disturbance magnitude would enhance the potential for equilibrium.

The thermal analysis in Section 2 revealed that the CFME aluminum walls will conduct much of the absorbed heat input to the liquid. This will serve to maintain liquid and vapor phases near the same temperature.

Since near-thermal equilibrium conditions are expected for the CFME mission, it is valid to compare the baseline and alternate TVS configurations on this basis.

3.2.1 VCS THERMAL MASS INFLUENCE. A major advantage of the baseline CFME insulation configuration over the alternate approach is the vapor-cooled shield (VCS) which enables venting of a high enthalpy vapor (i.e., a high vent gas temperature). As a result, a lower vent mass flowrate is required to maintain constant pressures in a given heating environment, as illustrated by Figure 3-2.

Unfortunately, a major disadvantage of the baseline configuration can also be the VCS, especially for short mission durations (approximately seven days in length). This disadvantage is due to the VCS stored energy at tank lockup, which will be released to the propellant during CFME cooldown. Figure 3-3 compares propellant heat input for both the baseline and the alternate insulation systems. The alternate system heat input curve was obtained by integrating the transient heating curve of Figure 2-4 and extrapolating to a duration of seven days. Figure 2-4 includes only radiation heat input since all penetration heating is intercepted by HX-1. It was assumed that the steady-state heating rate of 2.89 watts (9.86 Btu/hr) was established in 40 hours. The baseline configuration heating curve was obtained by dispensing the VCS stored energy at lockup (216 watt-hr, 737 Btu) over the 40-hour transient heating period. Note that VCS stored energy represents about 32 percent of the total energy input to the propellant during the seven-day mission. This is a substantial heat input quantity that detracts from VCS high thermal performance during steady-state operation.

It should be noted that this disadvantage of the baseline CFME could be lessened and perhaps eliminated by modifying the ground hold timelines and operations. For example,

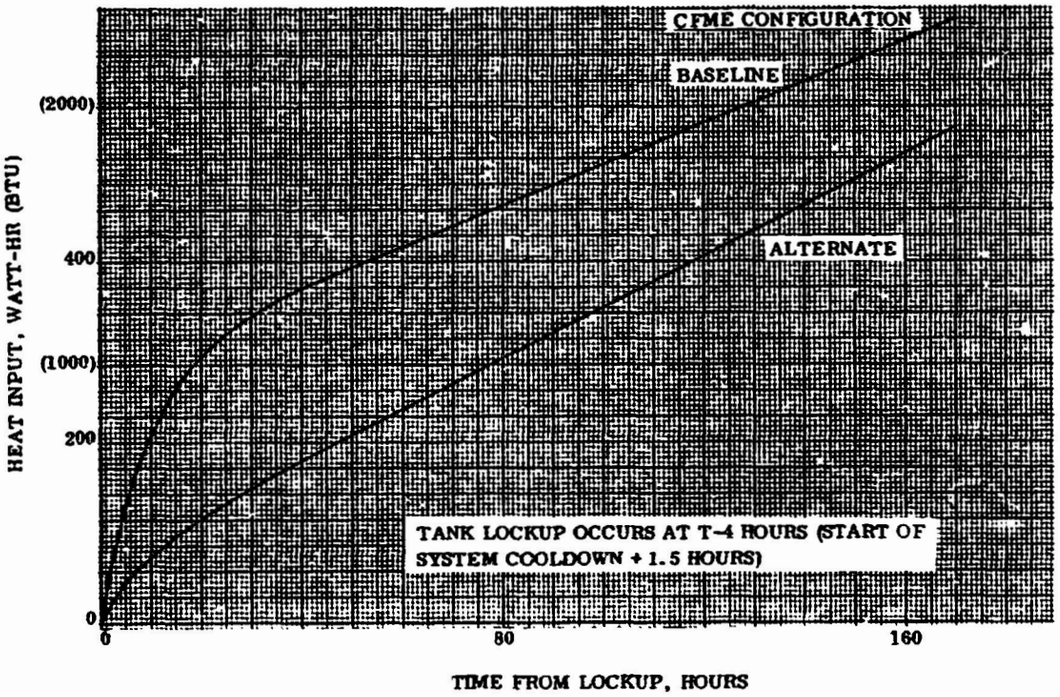

Figure 3-3. Radiation Heat Input to Propellants

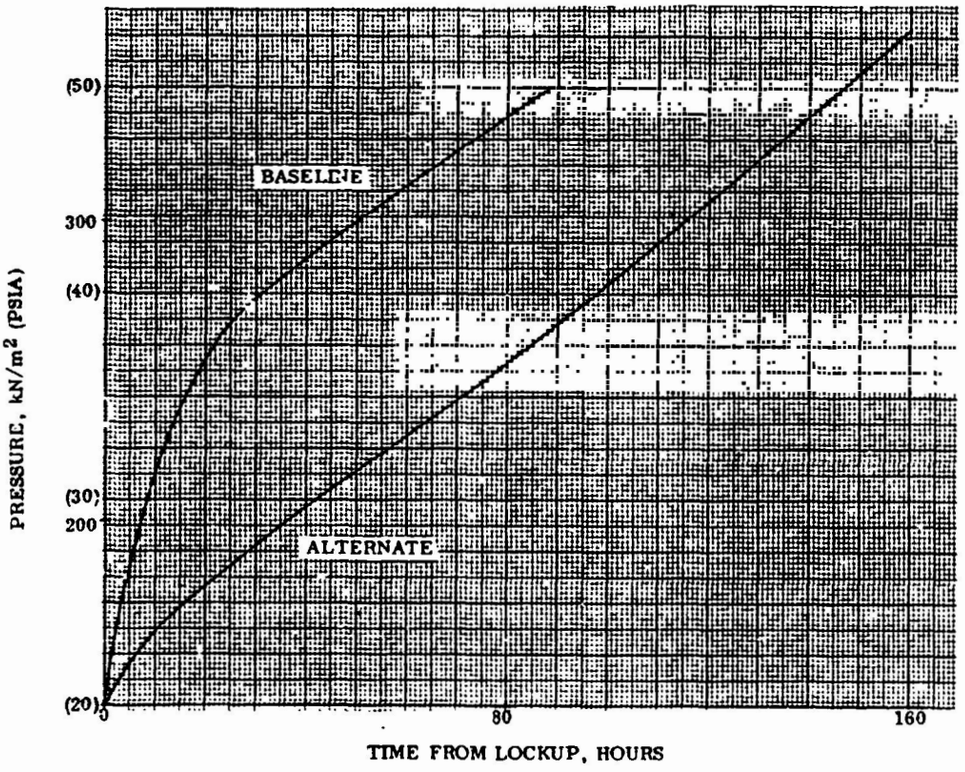

Figure 3-4. Comparison of Thermal Equilibrium Pressures During Mission

if cool fluid was flowed through the VCS for a sufficient time prior to tank lockup in order to remove some of the stored thermal energy in the VCS, it is probable that the rates of pressure rise for the baseline and the alternate system would be similar.

3.2.1.1 Thermal Equilibrium Pressure Histories. CFME vessel pressures were determined for the heating environments identified above. Results for the condition of HX-2 remaining inactive throughout the mission are given in Figure 3-4. Note that pressure rise rate during cooldown will be substantially greater for the baseline configuration than for the alternate. Even following cooldown, baseline pressures will remain at least 69 kN/m^2 (10 psi) above pressures for the alternate configuration. It is also seen that the alternate configuration could maintain pressures below the maximum allowable of 413.7 kN/m^2 (60 psia) with only HX-1 operating; baseline pressures would exceed the maximum allowable pressure if HX-2 did not operate.

3.2.2 MLI OPTIMIZATION OF ALTERNATE NO. 1. A task identified for this study was MLI system optimization for the alternate CFME configuration. The baseline CFME configuration was designed with 75 MLI layers outboard of the VCS. Since the VCS would be eliminated from the alternate design, additional MLI (up to a total of 105 layers) could be installed if required.

The method selected for optimization was to minimize total system weight. The variables considered are contained in the following expression

$$W_T = W_{MLI} + W_{HX} + W_{V1} + W_{V2} \tag{12}$$

where

W_T = total weight

W_{MLI} = MLI weight (obtained from Figure 2-3)

W_{HX} = HX-? weight (obtained from Figure 4-3)

W_{V1} = hydrogen mass vented through HX-1 during mission

W_{V2} = hydrogen mass vented through HX-2 during mission

HX-1 vented mass is determined by

$$W_{V1} = \dot{m}_{V1} \times \text{TIME} \tag{13}$$

where

$\dot{m}_{V1}$ = 0.0323 kg/hr (0.0712 lb/hr), from Table 3-1

TIME = 172 hours, from lock-up to end of mission

Since W_{V1} is a constant, total vent time is fixed and HX-1 is sized to intercept the penetration heat rate identified in Table 3-1.

The mass vented through HX-2 is determined by

$$W_{V2} = \dot{m}_{V2} \times \text{VENT TIME} \tag{14}$$

where

$\dot{m}_{V2}$ = f (radiation heat rate, Figure 2-2 and Figure 3-2)

VENT TIME = time from start of vent pressure control to end of mission

VENT TIME is a function of propellant heating rate and vent pressure control level.

Total mass, W_T, is plotted in Figure 3-5 as a function of MLI layers, from 76 to 108 layers; included also are the weights of each element. A vent pressure of 241 kN/m^2 (35 psia) was selected. It is noted that the MLI blanket weight increase exceeds the corresponding reduction in HX-2 vent mass and HX-2 weight (HX-2 weight was assumed directly proportional to design heat rate). Results show that the MLI system will optimize at about 76 layers.

Calculations were also performed to determine if vent pressure would influence optimization of the MLI system. Figure 3-6 results indicate that the optimum design point remains at 76 layers of MLI. This figure does show that total weight (W_T) can be reduced by about 1.1 kg (2.5 lb) if vent pressure level is increased to 310 kN/m^2 (45 psia) from 241 kN/m^2 (35 psia).

The design condition selected for the alternate CFME configuration will include a 76-layer MLI blanket. However, an earlier estimate of 84 layers, which had been made for the CFME, was used for the thermal analysis of Section 2. Since there is less than 0.1 kg (0.22 lb) difference between the two MLI configurations, the original 84-layer selection is considered acceptable as an optimum MLI design point.

3.3 CFME VESSEL PROPELLANT PRESSURE CONTROL

A detailed comparative evaluation of propellant pressure control for the CFME baseline and alternate configuration was beyond the scope of this study. Such a comparison would only be possible if detailed thermal performance predictions of the baseline configuration were available. A comparison was made, however, for the assumption of thermal equilibrium conditions existing during the mission (Section 3.3.1). Furthermore, a detailed analysis was conducted on the alternate configuration for two widely differing conditions, minimum and maximum ullage. These analyses and results are discussed respectively in Sections 3.3.2 and 3.3.3.

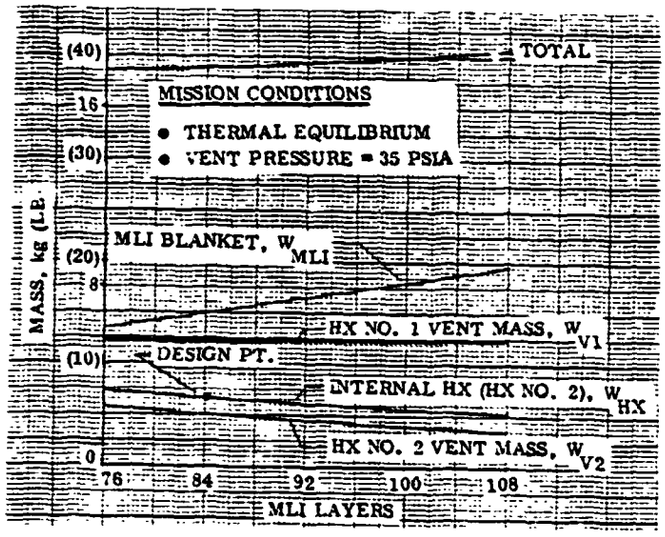

Figure 3-5. MLI Optimization of Alternate CFME Configuration

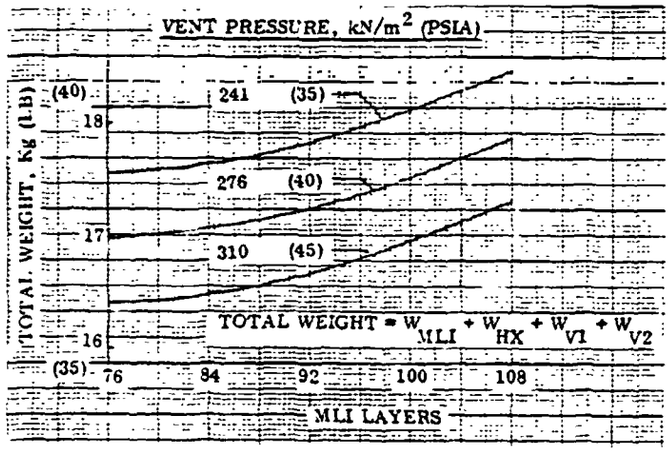

Figure 3-6. CFME Vent Pressure Level Will Have a Negligible Influence Upon MLI System Optimization

3.3.1 PRESSURE CONTROL COMPARISON (THERMAL EQUILIBRIUM CONDITIONS). An analysis was conducted to determine the adequacy of propellant tank pressure control for both the baseline and alternate configurations. Pressure control is more difficult to maintain during the CFME transient cooldown period because the higher propellant heating rates may exceed HX-2 capacity. Figure 3-7 shows CFME pressures for two HX-2 design flow conditions; 100 percent and 150 percent of steady-state heating. Propellant tank heating is described by Figure 3-3, and HX-2 is operated to control pressure to 241 kN/m^2 (35 psia). Figure 3-7 shows that pressure for the baseline configuration will rise above the control level for both heat exchanger flow conditions. The lower vent flow design condition will allow pressure to increase to 262 kN/m^2 (38 psia) by lockup plus 40 hours before pressure control is achieved. Pressure decay below 262 kN/m^2 (38 psia) will not occur because vent flow capacity is just balanced by the steady-state heat input. Pressure control at 241 kN/m^2 (35 psia) will be achieved if HX-2 is designed to intercept 150 percent of steady-state heat input. Pressure will increase to 252 kN/m (36.6 psia) for this case, before control is achieved.

In contrast to the above, pressure control for the alternate configuration will be achieved with both HX-2 vent flow design conditions. The 100 percent of design case will just maintain control pressure with no margin for pressure reduction. The 150 percent of design case will readily control pressure within any convenient band of operation.

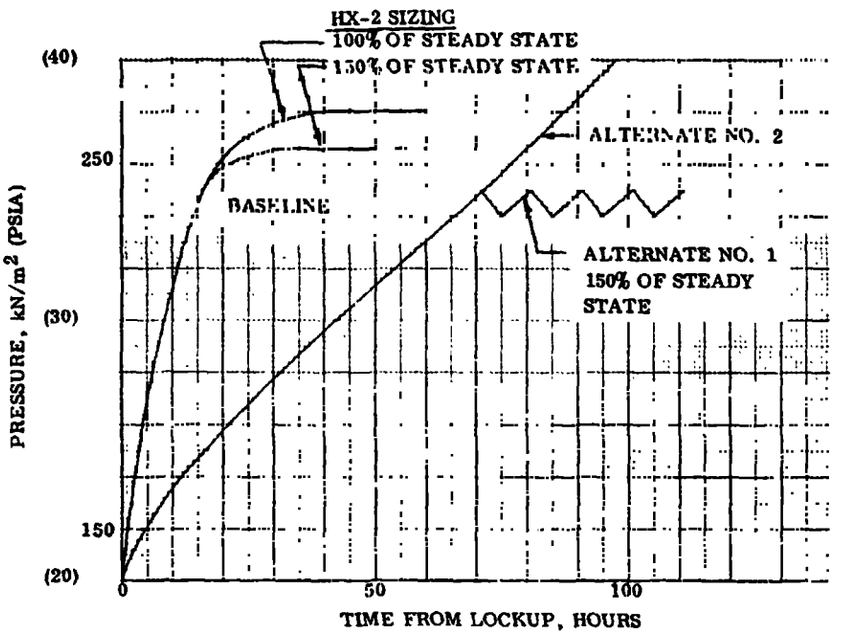

Figure 3-7. Comparison of Pressure Control for Baseline and Alternate Configurations

It is emphasized that the differences in pressure control capability indicated in Figure 3-7 are not due to HX-2 design differences between the baseline and alternate configurations. Rather, the improved pressure control capability for the alternate configuration is credited to removal of the VCS with its thermal mass. Furthermore, it is likely that the alternate design will provide more rapid rates of pressure reduction than will the baseline system since it removes heat directly from the contained fluid, whereas the baseline system attempts to control the rate of tank heating.

3.3.2 MINIMUM ULLAGE MODEL. The miminum ullage model selected for analysis includes three assumptions that will produce pessimistically high CFME pressures during the zero-g period. These assumptions are:

1. Heat transfer to the propellant is by conduction only. A thermal model is shown in Figure 2-10.

2. The ullage bubble is located a maximum distance from HX-2, which is internally mounted to the tank wall (Figure 2-17).

3. Tank pressure was selected to be the same as liquid Node No. 1 vapor pressure. This node is in contact with the tank wall and is a maximum distance from HX-2.

The implications of each assumption is considered in greater detail in the following sections.

ORIGINAL PAGE IS
OF POOR QUALITY

3.3.2.1 Conduction Heating. The thermal model of Figure 2-10 was employed to determine propellant temperature histories throughout the mission. A detailed description of the heat conduction model is provided in Section 2.5. The discussion in this section focuses on why the conduction assumption is conservative.

There are two factors that will tend tc dominate the propellant heating environment during the CFME mission: g-jitter and boiling heat transfer. G-jitter, as described in Section 3.2, will periodically occur throughout the mission at disturbance levels as great as 10^{-3} g's. It seems likely that each disturbance will tend to destroy any temperature gradient existing within the propellants. Furthermore, such disturbances would tend to mix the liquid and vapor phases.

Boiling heat transfer will also tend to de-stratify liquid temperature gradients. Heat conduction from the pressure vessel will create a warm liquid layer adjacent to the tank walls, while the interior fluid resides at a subcooled condition. Wall-boiling will occur once liquid has been heated to its boiling point. Bubbles generated by the boiling process will expand into the cooler liquid regions and condense. This condensation process will heat the inner regions of liquid more rapidly than if conduction alone were the mechanism. Again, the tendency will be for a reduced temperature gradient.

3.3.2.2 Ullage Bubble Location. Propellant tank pressure will be controlled by heat transfer to or from the ullage volume. Vessel pressure decay will occur when the ullage is chilled by HX-2, which acts as a low temperature heat sink for the liquid and vapor. HX-2 influence upon the ullage will be minimized if the separation distance is a maximum, therefore pressure control will be more difficult to achieve.

3.3.2.3 Tank Pressure/Vapor Pressure Relationship. Liquid adjacent to the tank walls will be warmer than the inner fluid elements. Furthermore, a liquid node located a maximum distance from the heat exchanger will be influenced less than one adjacent to HX-2 during operation. Because liquid node No. 1 represents the warmest possible liquid element within the pressure vessel, its vapor pressure will be the maximum. By assuming that node No. 1 liquid vapor pressure is the same as tank pressure, we guarantee that tank pressure will also be the maximum possible.

3.3.2.4 Predicted CFME Vessel Pressure History. CFME vessel pressures were determined for the selected propellant orientation of Figure 2-10. The MLI heating rate of Figure 2-4 was imposed upon the pressure vessel nodes. The analysis was set-up with HX-2 being controlled by the Node 1 temperature. The control limits were 23.6 to 23.72K (42.48 to 42.70R), which corresponds to a vapor pressure range of 241 to 248 kN/m^2 (35 to 36 psia). HX-2 was commanded on at the upper limit and extracted energy at the rate of 4.33 watts (14.79 Btu/hr).

Thermal analysis results are given in Figure 2-11, 2-12 and 2-13 for Node 1, Node 3, and the ullage node, respectively. The starting point for this analysis was taken at SSME shutdown. It was assumed that thermal equilibrium conditions would be established by

the main engine shutdown disturbances. Thermal equilibrium pressure at this time will be 151.7 kN/m^2 (22 psia), as determined from Figure 3-4. Vessel pressure histories were calculated by converting fluid node temperatures to their corresponding vapor pressures. Results are summarized in Figure 3-8 for the HX-2 heat removal rate of 4.33 watts (14.79 Btu/hr). Fluid node vapor pressure implications are discussed below.

Liquid Node 1. This node will experience the maximum vapor pressure increase in a pure conduction environment. The node will experience a rapid pressure increase immediately after SSME shutdown, as heat is transferred from the aluminum vessel walls. Although vapor pressure rise rates will substantially decrease with time, Node 1 pressure will remain above the thermal equilibrium pressure history until pressure control is initiated at shutdown plus 68 hours. Figure 3-8 shows that Node 1 pressure will exceed the thermal equilibrium pressure condition by about 6.9 kN/m^2 (1 psid) at the time pressure control is initiated with HX-2. The two pressures will become equal during the first vent cycle, and will remain equal throughout the pressure control period of flight.

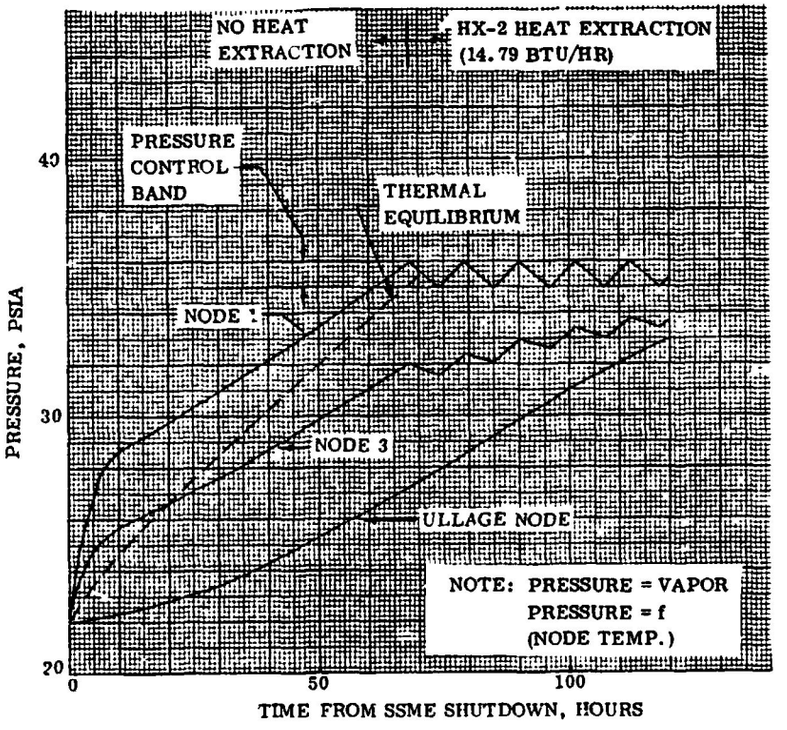

Figure 3-8. Predicted CFME Vessel Pressure History (Alternate Configuration No. 1)

Liquid Node 3. This node is in close proximity to Node 1, separated only by Node 2. Its vapor pressure will remain below that of Node 1 because it will not receive direct heat input from the tank walls. Vapor pressure rise rates will be the same for Nodes 3 and 1 from shutdown plus 30 hours until HX-2 is first activated at plus 68 hours. A 27.9 kN/m^2 (4 psid) vapor pressure difference will be maintained during this period. This difference will decrease to about 11 kN/m^2 (1.6 psid) by SSME plus 120 hours (the thermal analysis was terminated at plus 120 hours) because Node 3 pressures will continue to increase during pressure control cycling whereas Node 1 pressure will be limited between 241.3 and 248.2 kN/m^2 (35 and 36 psia).

Ullage Temperature Node($\dot{Q} = 0$). The ullage temperature node is a weighted average of the liquid interface nodes (5, 15, ···). The resulting vapor pressure is lower than the thermal equilibrium pressure because these nodes are protected from direct contact

with the tank skin where the warmest liquid nodes reside. This node pressure will remain below that of Node 3, although the difference will be only 4.1 kN/m^2 (0.6 psid) by SSME shutdown plus 120 hours. Note also that this node will not respond to the periods of HX-2 inactivity and operation as do Nodes 1 and 3.

3.3.2.5 Conclusions. Three important conclusions can be drawn from the thermal and thermodynamic analysis of the minimum ullage condition.

1. Pressure control is feasible with an internally-mounted heat exchanger.

2. A narrow pressure control band will be possible because fluid temperatures will respond very rapidly to the cooling influence of HX-2 when it is operating.

3. Even with this pure conduction model, it appears that fluid temperature variations will not be significant during the CFME mission. In fact, Figure 3-8 indicates that uniform fluid temperature conditions will be approached at times beyond SSME shutdown plus 120 hours.

3.3.3 MAXIMUM ULLAGE MODEL. Propellants will be expelled from the CFME during the latter stages of its seven-day mission. The possibility exists that segments of the pressure vessel will become dry as the ullage volume increases. The percent of dry wall area will depend upon propellant quantities expelled, and g-environment (Figure 3-9). A dry wall condition could result in excessive pressure rise rates if energy were conducted directly into the ullage rather than to the liquid as will occur for the minimum ullage condition. Because of this concern a thermal analysis (described in 2.6) was conducted to determine what the direct ullage heating rates would be, and if pressure control could be maintained during HX-2 operation.

Boundary conditions and assumptions for the model (Figure 2-16) were selected to increase the possibility of ullage heating. This would provide a more severe assessment of HX-2 pressure control capability. The following conditions were imposed upon this analysis:

1. Liquid volume = 25 percent of total volume.

2. A flat liquid-vapor interface results in a 87.5 percent dry wall area.

3. The liquid is positioned at the wall opposite the HX-2 location.

4. No heat exchange is allowed between liquid-ullage and ullage-heat exchanger surfaces.

5. HX-2 is cycled to maintain vessel pressure at 310 kN/m^2 (45 psia). Liquid and vapor are at the saturated temperature of 24.07K (44.5R) at the start of HX-2 operation.

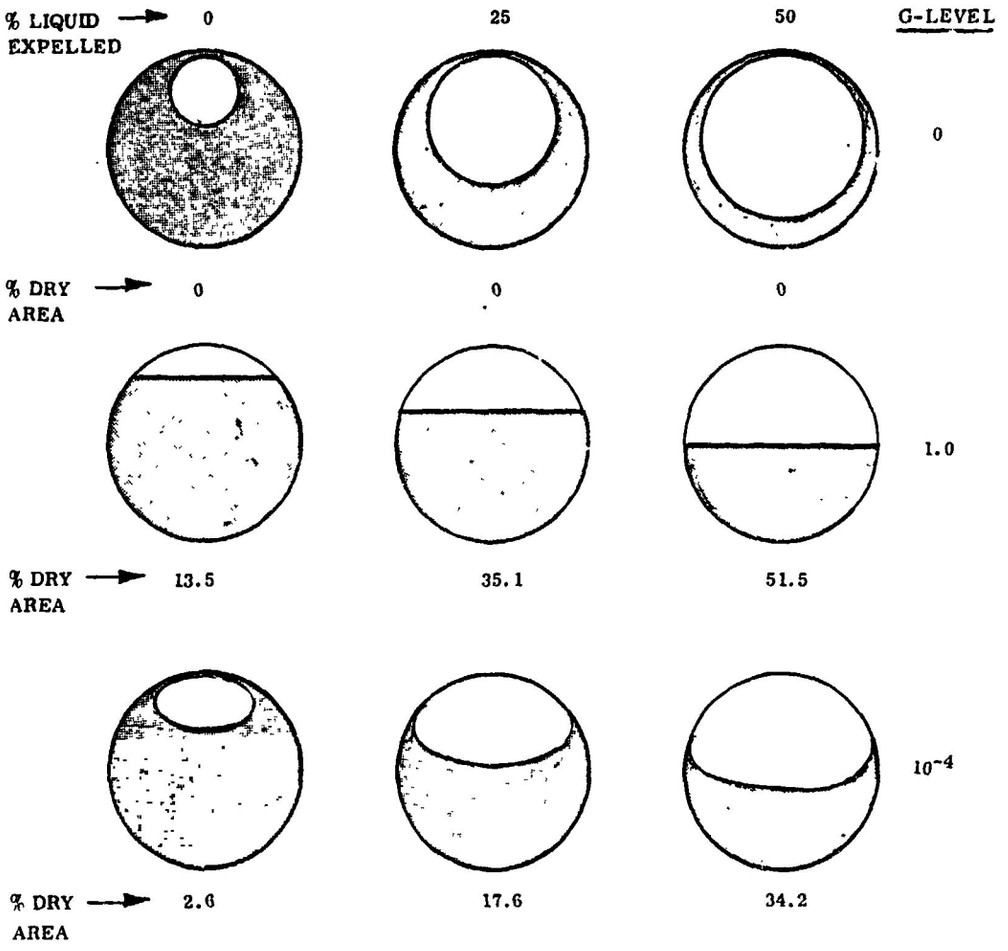

Figure 3-9. Steady-State Propellant Orientation Within CFME is a Function of Propellant Quantities and G-Level

Fluid cooling can occur only by (a) conduction from liquid to HX-2 along the aluminum shell, and (b) vapor condensation on the vessel wall if temperatures reside below the saturation vapor temperature.

Analysis results (given in Figure 2-16) showed that the entire dry wall area would reside at temperatures below saturation. This condition was due to the heat sink effect of HX-2 which maintained a sink temperature of 20.83K (37.5R) during operation. The low temperature condition will enhance pressure control in two respects. First, heat conduction to the ullage will not occur because all absorbed energy is conducted to HX-2. Second, vapor condensation will occur at the walls, removing ullage energy in the process. The net effect will be that of energy removal from the propellant which will result in a tank pressure decay.

Although a pressure control analysis was not performed on this model, it was evident that pressure control would be satisfactory. This judgment is based upon the expectation that substantial pressure vessel surface area will be available for vapor condensation. This direct means of ullage energy removal should quickly reduce ullage pressure.

3.3.3.1 Conclusions. The high thermal conductivity of the pressure vessel aluminum walls will serve to maintain near-thermal equilibrium fluid conditions while HX-2 is operating. Even for the extreme case of substantial dry wall areas, all incident heat flux will be intercepted by the wall and conducted to HX-2. Furthermore, vapor condensation is expected to occur at the tank walls because the entire dry wall surface will be subcooled relative to the saturated ullage temperature.

4

SYSTEMS COMPARISON

In this section a comparison is made of the baseline and alternate CFME configurations in terms of the following variables:

Comparative Weight
Costs
Complexity
Reliability
Performance

By necessity the comparison must be considered tentative due to (1) the preliminary nature of the HX-2 design, and (2) the unavailability of certain design details of the baseline configuration. This comparison is made in Section 4.2. It was necessary first to prepare preliminary design drawings of the internal heat exchanger installation (described in Section 4.1) and to analyze system performance, results of which were presented in Section 3.

4.1 CONCEPTUAL DESIGN OF INTERNAL HEAT EXCHANGER (HX-2)

The Cryogenic Fluid Management Experiment (CFME) consists of systems necessary to store and expel LH_2 in a low-g environment and to measure the performance of these systems. Martin Marietta Corporation has developed a conceptual baseline design which is basically a vacuum-jacketed tank equipped with an acquisition system and a thermal control system. The thermal control system for this baseline design incorporates a vapor cooled shield located concentrically between the tank and the vacuum jacket. A multilayer insulation (MLI) is mounted on the vapor cooled shield. The purpose of this effort is to replace the baseline vapor-cooled shield with an internal heat exchanger system as shown in Layout No. 26, (Figures 4-1, 4-2 and 4-3).

Layout No. 26 is a three sheet drawing showing the relationships between the heat exchanger, the tank and the acquisition system. Also included are heat exchanger construction details and a parts list with weights. Referring to Figure 4-1, the heat exchanger is a spherical segment assembly located at the bottom of the tank and straddling the channel type acquisition system at four places (see View C-C). The assembly is welded to the inside surface of the tank wall at the inside and outside perimeters (see view B-B and Detail "D").

Weld lands are added to the outside tank surface and the continuous fillet weld attachments shown in View B-B and Detail "D" of Figure 4-1 provide heat paths between the

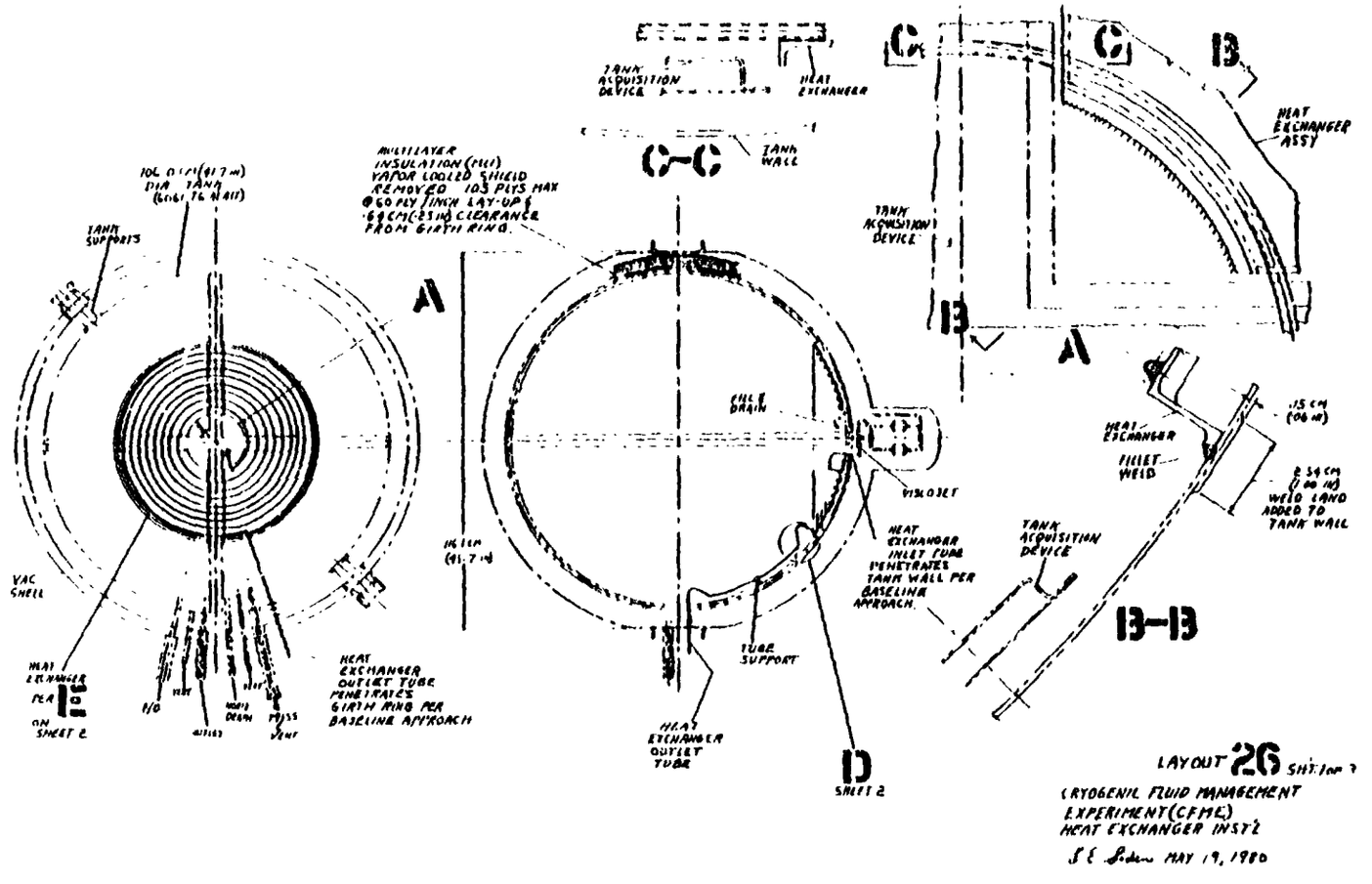

Figure 4-1. Internal Heat Exchanger Design Details

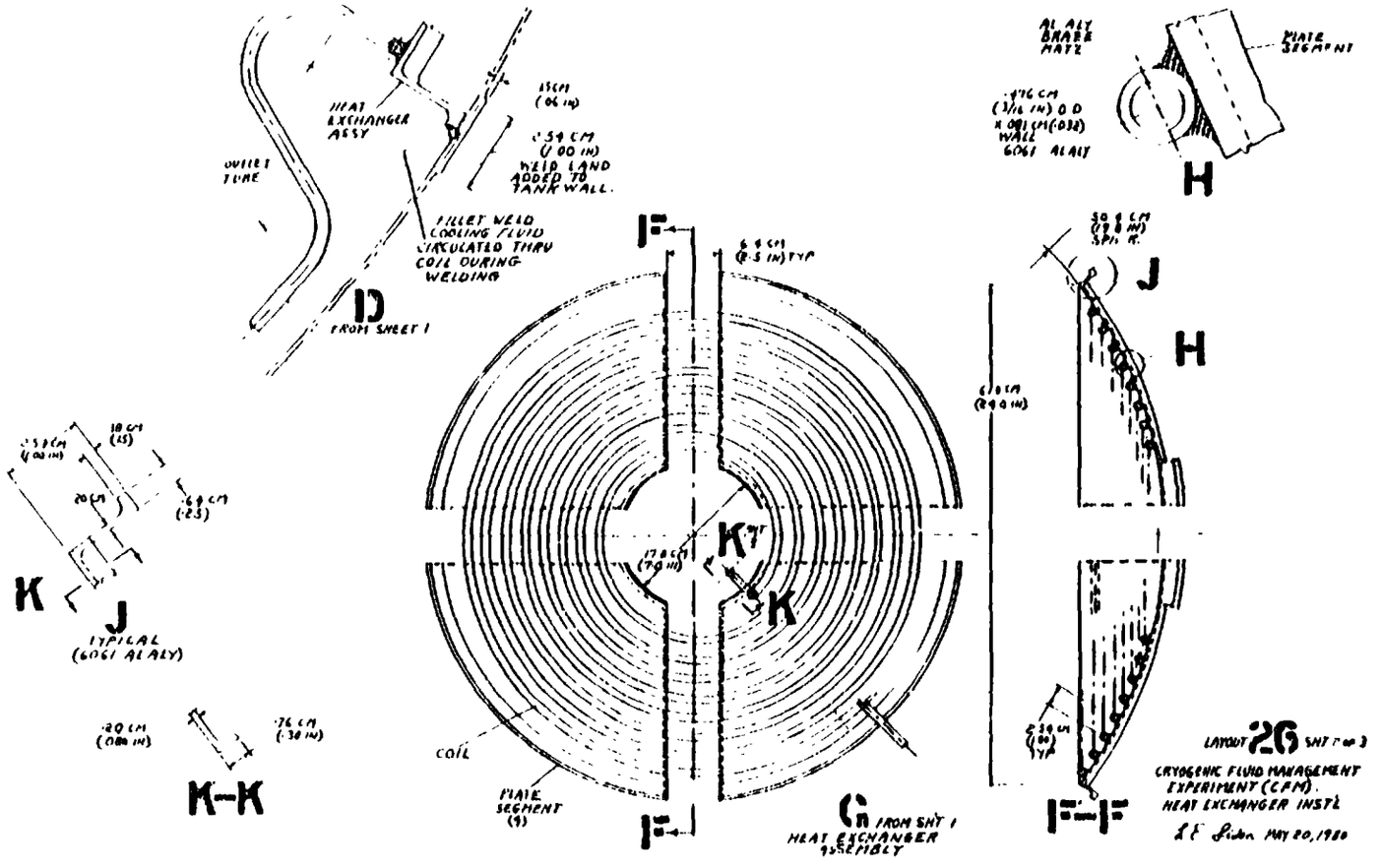

Figure 4-2. Internal Heat Exchanger Design Details

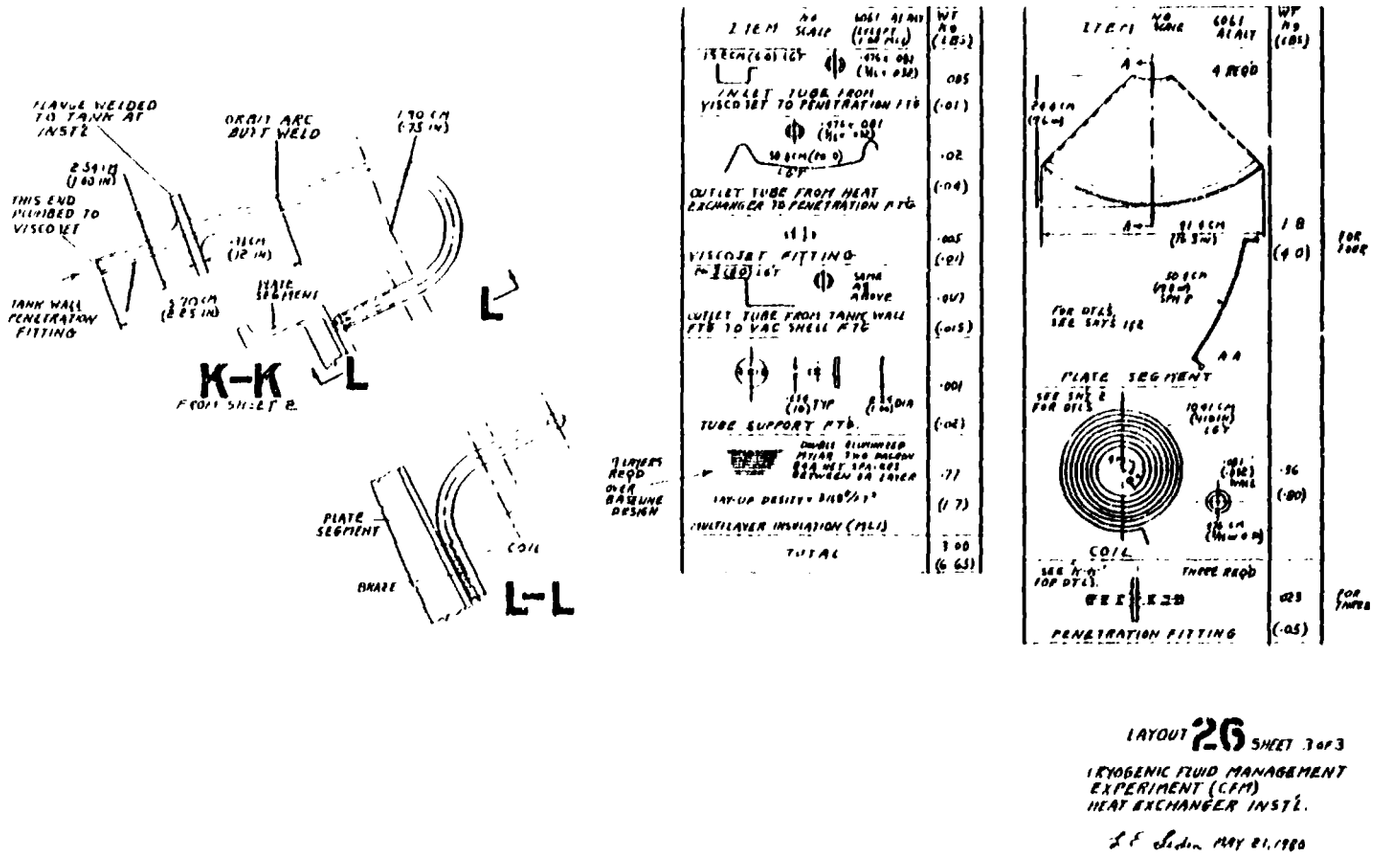

Figure 4-3. Internal Heat Exchanger Design Details

tank wall and heat exchanger. The heat exchanger is supplied with liquid from the acquisition system outlet through a "viscojet" and a short tube section which connects to a tank wall penetration fitting shown in View "K-K" on Sheet 3 of the layout. For the outlet side, a second tube section is routed inside the tank to a penetration fitting located near the girth area. This outlet circuit is completed with a third tube section which interconnects the tank wall and vacuum shell penetration fittings.

The heat exchanger assembly consists of four plate segments, one tubular spiral coil and an inlet fitting. The material is 6061 aluminum alloy. Each plate segment is a spherical surface with two "L" shaped flanges at the inside and outside radii and two stiffener webs along the sides (see detail "J" and view "K-K"). The four segments are machined from a single spherical piece which has been shaped by spin, drop, or explosive forming processes.

The heat exchanger coil is a continuous tube wound into a spiral which conforms to the spherical shape of the plate segments. The inlet and outlet terminals have "U" bends for plumbing connections. The inlet terminal is equipped with a spool type penetration fitting shown in view "K-K." When the heat exchanger assembly is positioned in the tank, the flange portion of this penetration fitting is engaged with a hole in the tank wall and welded from the outside. The weld between the penetration fitting and coil terminal indicated in view "K-K" is made at the bench level.

The coil is continuously brazed to the plate segments as shown in detail "H" of the layout. This is accomplished by clamping the parts in a holding fixture and applying the dip brazing process.

4.1.1 HX-2 WEIGHT BREAKDOWN. The configuration and weight of each part is shown in Sheet 3 of the layout. Excluding the MLI layers, approximately 15 parts are required including a tube support clamp and bolt/nut set not shown. The three penetration fittings shown include one for the vacuum shell penetration. Exact routings for the inlet and outlet tubes are not included on the layout, therefore the lengths and configurations indicated are approximate. The nine layers of MLI shown is the additional requirement over the baseline design.

4.1.2 FABRICATION CONSIDERATIONS. The vapor-cooled shield is a thin-walled sphere equipped with a heat exchanger coil. The shield completely envelopes the tank and also serves as the mounting surface for the MLI. A spacing is provided between tank and shield; this installation requires minimum thermal contact with the tank wall. The system selected for the baseline design supports the shield from the tank trunnions. Spacer lands are also provided at the tank girth area which acts as mid-span supports. To permit assembly, the shield must be installed in two halves with provisions for inter-connecting the heat exchanger tubes and the shells. In general, a vapor-cooled shield will result in penalties in weight, fabrication and cost. The design shown in Figures 4-1 through 4-3 reduces these penalties by using a small rigid heat exchanger attached directly to the inside of the tank wall. Moreover, there will be a greater

impact upon the pressure vessel for the internal HX design. For example, the heat exchanger flanges and penetration fittings are welded to the tank wall with the acquisition system installed. This requires a high degree of quality control and protection procedures for the acquisition system.

4.2 VCS VERSUS INTERNAL HX, RELATIVE EVALUATION

A critical comparison of the baseline TVS and an alternate system employing an internal HX is summarized in Table 4-1. The major conclusions of this comparison must be regarded as tentative, for the following reasons:

1. The preliminary conceptual level of design of the internal HX installation of Figures 4-1, 4-2 and 4-3.

2. The general unavailability of design details of the baseline TVS system.

4.2.1 COMPARATIVE WEIGHT. Based on a cursory comparison of the gross dimensions of the respective systems, it is observed that because of its smaller size, the alternate system (Internal HX) would comprise a weight reduction from baseline TVS levels. Estimated weights of the subcomponents peculiar to the alternate system are contained in Figure 4-3. This total weight of 3.0 kg (6.65 lb) compares very favorably to the VCS weight of 8.6 kg (19.0 lb). It is anticipated that relative weight will not be a strong discriminator in evaluating the respective systems.

4.2.2 MATERIAL COSTS. Again, because of its smaller size, the alternate system would entail lower material costs. This discriminator would also be of secondary importance.

4.2.3 FABRICATION COSTS. Apparent differences in probable fabrication methods are few. Anticipated handling and tooling details are dissimilar, and appear to slightly favor the internal HX. Furthermore, the internal HX would probably not require heat treat following dip braze attachment of the tubing coils to the plate segments. This may constitute an advantage of the alternate system, since post-fabrication heat treatment of the VCS may be necessary.

4.2.4 DEVELOPMENT COSTS. The alternate system performance predictions from this study suggest a very strong functional design, i.e., internal HX performance is not at all contingent on adherence to rigorous dimensional constraints. Although similar evaluation of the baseline TVS was not possible, the forgiving design of the alternate system is thought to be an advantage favoring reduced development costs.

4.2.5 INSTALLATION COMPLEXITY. As noted in Table 4-1, complexities in the respective installations are not similarly located. The internal HX must be welded in place following installation of the acquisition device, and this would appear to be

Table 4-1. Baseline TVS/Alternate No. 1 Comparison Matrix

3 — PREFERRED CONCEPT
2 — APPARENT EQUIVALENCE
1 — INFERIOR CONCEPT

ITEM	VAPOR-COOLED SHIELD	ALTERNATE NO. 1 (INTERNAL HX)
WEIGHT	1	3
MATERIAL COSTS	1	3
FABRICATION COSTS (1)	2	2
DEVELOPMENT COSTS (2)	1	3
INSTALLATION COMPLEXITY (3)	1	3
RELIABILITY (4)	1	3
PERFORMANCE (5)	3	1
	10	20

TRADE ITEMS

(1) FABRICATION COSTS: SIMILAR METHODS EMPLOYED, MAJOR DIFFERENCES ONLY IN COMPONENT SIZE AND HANDLING DETAILS.

(2) DEVELOPMENT COSTS: INTERNAL HEAT EXCHANGER IMPOSES NO RIGOROUS DIMENSIONAL CONSTRAINTS, FUNCTIONAL DESIGN IS STRONG, NO IDENTIFIABLE WORRY ITEMS.

(3) INSTALLATION COMPLEXITY: RESPECTIVE COMPLEXITIES ARE NOT SIMILARLY LOCATED. HOWEVER, INTERNAL HX PERMITS MAJOR INSTALLATION AND LEAK CHECKS PRIOR TO PRESSURE VESSEL CLOSE-OUT WELD, WITH NO SUBSEQUENT HANDLING.

(4) RELIABILITY: CLOSE-COUPLED, DURABLE INTERNAL HX LESS SUBJECT TO LEAKAGE. LEAKAGE INTO HX POSES NO PROBLEM. LEAKAGE OUT OF VCS CAN COMTAMINATE MLI, CAUSING EXPERIMENT FAILURE.

(5) PERFORMANCE: HIGH VCS EXIT TEMPERATURE RESULTS IN A LOWER VENT MASS FOR MISSION.

the major complexity of the alternate systems. However, weld access is fully adequate, and leak checks can be performed prior to close-out welding of the pressure vessel. Subsequent steps in assembly of the alternate system would be greatly simplified with the absence of the VCS. It is tentatively concluded that reduced net complexity favors the alternate system.

4.2.6 COMPARATIVE RELIABILITY. Due to its reduced size, the internal HX is a durable, close-coupled installation, and can thus tolerate severe dynamic loading. Moreover, unlikely leakage into the internal HX would not penalize system performance. Conversely, leakage out of the VCS could be expected to seriously penalize experiment performance due to contamination and thermal shorting of the MLI. It is thus concluded that of the two system concepts, the alternate system offers greater reliability.

4.2.7 COMPARATIVE PERFORMANCE. Performance of the alternate CFME thermodynamic vent system (TVS) was discussed in Section 3. Performance of the two major functions of the TVS, pressure control capability and thermal performance is assessed. Analysis of the alternate configuration illustrated that HX-2 would be capable of providing satisfactory pressure control even under the extreme conditions evaluated. The excellent thermal contact between HX-2 and the propellant will enable a rapid vessel pressure reduction when HX-2 is operating. A similar pressure control analysis was not performed on the baseline CFME because of insufficient data. It does appear, however, that pressure control capability for the baseline VCS will be less than for the alternate configuration. This judgment is based upon the different thermal design approaches of the two configurations. Whereas the internal HX will be in close thermal contact with the propellant, the VCS HX-2 requires less thermal contact in order to intercept heat before it is absorbed by the propellants. This reduced thermal contact would reduce the propellant energy extraction rate and, consequently, will reduce tank pressure decay rates.

The combined weights of the TVS and vented masses were taken as a measure of system thermal performance. In this case, thermal performance increases as total weight is reduced. Total weight for the alternate configuration is given by Equation 3-12, and includes MLI and HX-2 weight, and total vent mass. Total weight data was given in Figure 3-6 as a function of MLI layers and CFME vent pressures. This data is plotted in Figure 4-4 as a function of vent pressure for the optimum MLI blanket configuration of 76 layers. The corresponding baseline configuration total weight is also given in Figure 4-4 for comparison. Baseline system total weight includes VCS weight, but does not include HX-2 weight since its value was not given. The baseline configuration weights are seen to be only slightly greater than for the alternate configuration. Consequently, performance of the two configurations is considered to be equivalent.

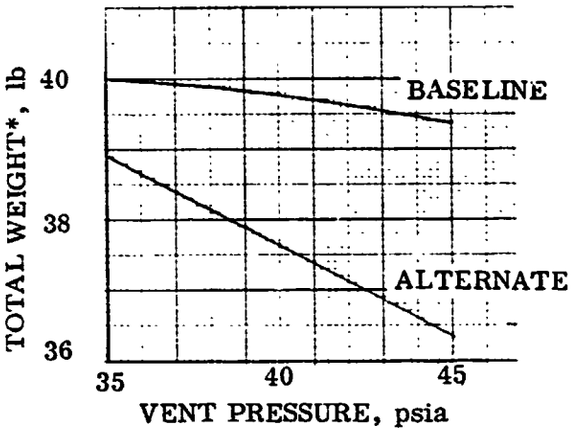

* Total Weight = $W_{MLI} + W_{HX-2} + W_{V1} + W_{V2}$ (Alternate)

= $W_{MLI} + W_{VCS} + W_{V1} + W_{V2}$ (Baseline)

Figure 4-4. TVS Weight Comparison

4.3 CONCLUSIONS

The TVS comparison which is summarized by Table 4-1 favors the internal heat exchanger configuration over the VCS. The following conclusions are made:

1. Performance. Either concept will perform satisfactorily during the seven-day mission. Advantages and disadvantages are such that performance should not influence system selection.

2. Complexity/Costs. An internally mounted heat exchanger represents a simpler configuration than a VCS from the standpoint of development, fabricaton, installation and complexity. This leads to the conclusion that development costs will be greater for the VCS. The absolute cost differential could not be determined because: (a) the internal HX design was too preliminary to estimate accurate costs, and (b) cost data was not available on the baseline configuration.

Based upon the above, the internal heat exchanger is recommended as a replacement for the vapor-cooled shield for the CMFE.

5

REFERENCES

1-1. Eberhardt, R. N., Tegart, J. R., "Conceptual Design Report, Cryogenic Fluid Management Experiment (CFME)," MCR-79-561, June 1979.

1-2. Gille, J. P., "Thermal Analysis Report, Cryogenic Fluid Management Experiment (CFME)," MCR-79-564, June 1979.

1-3. Tegart, J. R., "Hydrodynamic Analysis Report, Cryogenic Fluid Management Experiment (CFME)," MCR-79-563, June 1979.

2-1. O'Neill, R. F., Neuharth, E. R., "Convair Thermal Analyzer," Computer Program No. P4560, GDC-BTD69-005A, Contract NAS3-11811, 29 May 1969.

2-2. O'Neill, R. F., and Schappelle, R. H., "A Numerical Procedure for Solution of Radiation and Convection Fin Heat Transfer Problems," GDCA-BTD71-001, Contract NAS3-13504, April 1971.

2-3. Keller, C. G., "Thermal Performance of Multilayer Insulations," LMSC-A974469, NASA CR-72747, 20 April 1971.

2-4. Keller, C. W., et al, "Thermal Performance of Multilayer Insulations," LMSC-D349866, NASA CR-134477, 1974.

2-5. Sumner, I. E., "Thermal Performance of Gaseous-Helium-Purged Twin-Mounted Multilayer Insulation System During Ground-Hold and Space-Hold Thermal Cycling and Exposure to Water Vapor," NASA Technical Paper 1114, 1978.

2-6. Collier, J. G., "Convective Boiling and Condensation, McGraw-Hill, 1972.

	No. of Copies
National Aeronautics & Space Administration Lewis Research Center 21000 Brookpark Road Cleveland, OH 44135	
Attn: Contracting Officer,	1
E. A. Bourke, MS 501-5	2
Technical Utilization Office, MS 3-19	1
Technical Report Control Office, MS 5-5	1
AFSC Liaison Office, MS 501-3	2
Library, MS 60-3	2
Office of Reliability & Quality Assurance, MS 500-211	1
E. P. Symons, Project Manager, MS 501-8	5
T. H. Cochran, MS 501-8	1
E. J. Domino, MS 501-8	1
J. C. Aydelott, MS 501-8	1
E. W. Kroeger, M.S. 501-8	1
National Aeronautics & Space Administration Headquarters Washington, DC 20546	
Attn: RTP-6/F. W. Stephenson	1
RST-5/E. Gabris	1
National Aeronautics & Space Administration Goddard Space Flight Center Greenbelt, MD 20771	
Attn: Library	1
A. Sherman, MS 713	1
National Aeronautics & Space Administration John F. Kennedy Space Center Kennedy Space Center, FL 32899	
Attn: Library	1
National Aeronautics & Space Administration Ames Research Center Moffett Field, CA 94035	
Attn: Library	1
National Aeronautics & Space Administration Langley Research Center Hampton, VA 23365	
Attn: Library	1
National Aeronautics & Space Administration Johnson Space Center Houston, TX 77001	
Attn: Library	1
EP5/W. Chandler	1
National Aeronautics & Space Administration George C. Marshall Space Flight Center Huntsville, AL 35812	
Attn: Library	1
EP43/L. Hastings	1
EP43/A. L. Worlund	1
NASA Scientific & Technical Information Facility P. O. Box 8757 Balt./Wash. International Airport	
Attn: Accessioning Department	25